Theory of the Stark effect

David A. Harmin*

Department of Physics, University of Chicago, Chicago, Illinois 60637

(Received 26 January 1982; revised manuscript received 2 July 1982)

Theoretical photoabsorption cross sections for alkali-metal atoms in a static electric field F are derived for energies near the zero-field ionization threshold ($\epsilon = 0$), extending a previous development for hydrogen. Spectra result from *zero-field* dipole matrix elements and a density-of-states matrix $D_{l'l}^{F}$. The factors $D_{l'l}^{F} = (\langle \Psi' | \Psi \rangle^{-1})_{l'l}$ represent a renormalization of the photoelectron's wave function Ψ_l necessitated by the long-range Coulomb plus Stark potential. The matrix D^{F} contains all spectral information on quasidiscrete Stark levels and continuum resonances, expressed as an algebraic function of (1) quantum defects μ_l embodying core effects, (2) a frame transformation between spherical and parabolic coordinates in the pure Coulomb field outside the alkali-metal core, and (3) factors $H_{l'l}^{F}$ and $h_{l'l}^{F}$ calculated from asymptotic amplitudes and phases of *hydrogen-Stark* wave functions of the parabolic dissociation channels. Hydrogenic parameters are calculated semianalytically within the WKB approximation; μ_l and dipole matrix elements are known independently. Predicted cross sections for photoionization of the excited $3^{2}P_{3/2}$ state of Na agree with experiment. The theory reproduces (a) asymmetric resonances observed at $\epsilon < 0$, parametrized as a Beutler-Fano profile for a simple case, and (b) the oscillations observed at $\epsilon > 0$, attenuated by factors $\cos 2\pi\mu_l$ from their predicted depth in H. Dependences on light polarization are sorted out for two-photon excitation.

I. INTRODUCTION

Theoretical studies of the Stark effect of Rydberg spectra have traditionally focused on the shifts and broadening of the discrete levels of hydrogenic atoms photoexcited from the ground state. However, recent experiments performed on Rb,[1,2] Na,[3-5] Ba,[5] K,[6] and rare-gas atoms,[7] rather than H, have shown two additional effects in the photoionization cross section near the Rydberg series limits ($\epsilon = 0$): (i) A pronounced *asymmetry* in the profiles of the high-lying Stark levels, and (ii) a series of polarization-dependent modulations extending *beyond* the zero-field threshold. The asymmetric line shapes are evidently caused by interference effects between continuous and quasidiscrete channels that are coupled by a nonhydrogenic core. The resonances (ii) were discussed by Rau,[8] in the general context of external-field effects on Rydberg spectra near threshold. Subsequent explanations[9-11] have based their qualitative success on a hydrogenic model, whose potential (in atomic units)

$$V(\vec{r}) = -1/r + Fz \qquad (1)$$

also pertains to the region outside an alkali-metal ion core, $r > r_0 \sim O$ (1 a.u.). ($F = \vec{F} \cdot \hat{z}$ is a static uniform electric field.) The influence of the core has not previously been evaluated explicitly. The

present paper describes a theory, recently outlined elsewhere,[12] which combines the hydrogenic Stark problem with field-*in*dependent core effects and which reproduces the available alkali-metal spectra.

Our treatment of the nonhydrogenic Stark effect rests on the fact that the Coulomb term of the potential (1) overwhelms the Stark term whenever $r \ll F^{-1/2} \sim 1000$ a.u.[10,13] Since an alkali-metal core's electrons are confined within a radius $r_0 \sim O$ (1 a.u.), where the Stark field can be ignored, the photoabsorption process proper is adequately described by *zero-field* parameters, namely, quantum defects and dipole matrix elements of the relevant atom. These quantities can be obtained from experimental spectra[14] or *ab initio* calculations. The photoexcited electron, on the other hand, escapes to $z \rightarrow -\infty$ in the long-range potential (1) without regard to details of the ion core, whose potential departs from a pure Coulomb form only at $r < r_0$. Thus, the separate physical stages of photoabsorption and ionization are herded into separate regions of physical space.

The closed-shell core potential, though complicated, is spherically symmetric whereas the Schrödinger equation with the potential (1) is separable[15,16] only in parabolic coordinates (ξ, η, ϕ). The field axis destroys the spherical symmetry when $F \neq 0$, but invariance about the z axis is preserved

and m remains a good quantum number. Orthogonal parabolic eigenfunctions having $n_1 = 0,1,2,\ldots$ nodes in the bound ξ coordinate perform then a role analogous to that of Legendre polynomials having $l - m = 0,1,\ldots$ nodes. The common ground between the region of spherical $(r \ll F^{-1/2})$ and parabolic $(r \geq r_0)$ symmetry lies in the broad zone

$$r_0 \lesssim r \ll F^{-1/2} \text{ a.u. } , \tag{2}$$

wherein the potential is purely Coulombic and is therefore invariant under *both* symmetry groups.[16] In the range (2), the spherical-symmetry eigenfunctions of atomic processes at small r can be expanded into parabolic eigenfunctions appropriate to the long-range potential (1) (or vice versa). Note that the core occupies the region where *both* ξ and η are small. For this reason, the motion in ξ alone remains external to the core even at $\xi \sim 0$ (when ξ is not small), with unchanged n_1 quantization. The core acts only on the combined motion of ξ and η by mixing the parabolic channels and producing phase shifts in the η motion.

The Coulomb degeneracy in region (2) provides the necessary link between photoexcitation of a Rydberg electron and ionization in a Coulomb plus Stark field. The final state of atomic photoabsorption in this region is represented by a wave function $\Psi_{\epsilon lm}(\vec{r})$ normalized per unit energy, e.g., in a WKB approximation. This normalization would be appropriate to calculation of the photoabsorption cross section if $\Psi_{\epsilon lm}$ could be integrated to $r \to \infty$ in the absence of significant potential barriers. In the presence of the Stark field beyond region (2), $\Psi_{\epsilon lm}$ will instead be redistributed among parabolic continuum channels, each of which has its own density-of-states spectrum. The aggregate of these densities of states represents the capacity of the outer field for absorbing the photoelectron. This quantity will be seen to take the form of a density-of-states matrix, $D^F_{l'l}$, which serves to renormalize $\Psi_{\epsilon lm}$ per unit energy and thus to represent the effect of the outer field on photoionization. This matrix embodies all spectral information on the nonhydrogenic Stark effect through (1) parameters of the Coulomb-Stark wave functions (Sec. II), and (2) zero-field core effects represented by quantum defects $\mu_l = \delta_l / \pi$. In the total cross section, $D^F_{l'l}$ appears as a factor which simply modulates the *zero-field* oscillator-strength density. This density-of-states matrix is a novel concept which may find broad application.

The effect of an alkali-metal ion core will be in-

corporated as an element of the modulating factor D^F, whereas the electric field has generally been treated as a perturber of the zero-field Rydberg spectrum itself.[17] Theoretical aspects of hydrogenic cross sections are thus seen to contain most of the essentials for our treatment of alkalis. Earlier numerical calculations[9] on the ground-state photoabsorption by H in a Stark field have in fact reproduced the positions and spacing—though not the depth—of the threshold modulations observed in Na (Refs. 3—5) and Rb (Ref. 1). These structures have been rederived and interpreted semianalytically in a recent paper,[10] referred to as I. The general WKB methods of I are algebraically convenient and will prove sufficiently accurate for theoretical application to the observed alkali spectra.

The threshold modulations are predicted to occur in H (Refs. 8—11) for π-polarized light $(\parallel\vec{F}; m = 0 \to m = 0)$ but only weakly for $\sigma^{\pm}$-circularly polarized light $(\perp\vec{F}; m = 0 \to \pm 1)$. Each modulation corresponds to the threshold for a specific n_1 channel, i.e., to the energy required to reach that channel via photoexcitation of the ground state. The effect of the core is merely to attenuate the depth of the modulations, and possibly to invert them, without shifting their positions. However, the asymmetry of the sharp peaks below threshold (corresponding to quasibound Stark levels) cannot be reproduced in the hydrogenic model alone.

We also extend here the treatment of single-photon absorption to the two-step photoionization used in the experiments of Refs. 3—6. Specifically, we shall consider excitation of the ground states of H and Na through an intermediate np level. In two-step excitations, the photons may be polarized independently and we must account for various possibilities: $\pi\pi$, $\pi\sigma^{\pm}$, $\sigma^{\pm}\sigma^{\pm}$, $\sigma^{\pm}\pi$, $\sigma^{\pm}\sigma^{\mp}$. We shall find the polarization-dependent results to be qualitatively similar to those of single-photon ionization for both H and the alkalis. With reference to the intermediate and final states ψ_i and ψ_f, the threshold modulations are (1) large for $m_i = 0 \to m_f = 0$ $(\pi\pi)$ transitions and (2) very small for m_i and/or $m_f = \pm 1$. Generally, the modulations are larger as the value of $l - |m|$ in the *final* state is larger and, for given l, $|m|$ is smallest; the value of $l - |m|$ for the initial state is only of secondary importance, in contrast to the predictions of Ref. 9 based on the parity of $l_i + m_i$. In addition, ls coupling in a state ψ_i with $m_j = \frac{1}{2}$ and $j = \frac{1}{2}$ or $\frac{3}{2}$ allows the atom to reach different values of m_f for $\pi\pi$ and $\pi\sigma^{\pm}$ polarizations, thus superposing large and small modula-

tions, as well as sharp peaks below threshold with different profiles.

II. HYDROGENIC PARAMETERS FOR PHOTOEXCITATION

Our approach to photoexcitation of a Rydberg electron conforms to the multichannel quantum-defect theory,[18] which emphasizes the distinction between two regions of physical space and between the behavior of the eigenfunctions in these regions:

(1) An external region, $r \geq r_0$, where the combined Coulomb plus Stark potential Eq. (1) permits semianalytical solutions of the Schrödinger equation, sensitive to barrier and threshold effects.

(2) A localized core, $r \leq r_0$, where the Rydberg electron has a large kinetic energy and is therefore insensitive both to small variations of its total energy and to the presence of external fields. The matching of wave functions at the core boundary results in a coupling of the external solutions. This coupling will be described by a K matrix, whose diagonal form depends only on the quantum defects $\mu_l \equiv \delta_l / \pi$ of the (alkali-metal) atom.

In Sec. II A we describe the parameters which characterize the external parabolic eigenchannels for hydrogen in a Stark field F. We then apply a *coordinate transformation* in the region (2) (Sec. II B); here the external field is negligible as compared to the Coulomb field, which has both parabolic and spherical symmetry. The connection between the regions of different symmetry will prove central in factoring the total cross section into (a) a field-independent cross section and (b) a function representing the threshold modulations and broadened Rydberg levels induced by a finite Stark field for single- (Sec. II C) and two-photon (Sec. II D) excitation. The derivation of hydrogenic photoionization cross sections in Secs. II C and II D will contain all the essential ingredients for constructing nonhydrogenic cross sections.

We will view photoexcitation of a hydrogenic state $\psi_{\epsilon lm} \equiv \psi_l$ as taking place at $r \leq r_0$, as described in Sec. I. The frame transformation to the parabolic region at larger distances then serves to represent ψ_l as a superposition of continuum basis functions of the electron escaping in the potential (1). Orthonormalization of the set $\{\psi_l\}$ via the overlap matrix $\langle \psi_{l'} | \psi_l \rangle^{-1/2}$ determines the extent to which each photoexcited spherical function ψ_l is "absorbed" into the continuum. The Stark effect will thus be ultimately encapsulated in a *density-of-states* (DOS) *matrix*

$$D_{l'l}^F = [\langle \psi' | \psi \rangle^{-1}]_{l'l} \; .$$

This matrix replaces the DOS of the spherically symmetric wave functions, $\delta_{l'l}\delta(\epsilon' - \epsilon)$, determined by the photoabsorption process proper at small r, by the DOS of the continuum parabolic functions appropriate to ionization. This method will be readily extended (in Sec. III) to include the coupling of parabolic eigenchannels by a spherically symmetric, closed-shell ionic core; experimental or theoretical dipole matrix elements and quantum defects will appear as semiempirical input parameters.

A. Hydrogenic eigenfunctions

The Schrödinger equation for H ($Z = 1$) in a combined Coulomb-Stark potential $v(\vec{r}) = +Fz - 1/r$ is separable[19] in parabolic coordinates,

$$\xi = r + z = r(1 + \cos\theta) \; ,$$

$$\eta = r - z = r(1 - \cos\theta) \; .$$

The resulting equations for ξ and η (taking $m \geq 0$) are

$$\left[\frac{d^2}{d\xi^2} + \left[-\frac{m^2 - 1}{4\xi^2} + \frac{\beta}{\xi} + \frac{1}{2}\epsilon - \frac{1}{4}F\xi \right] \right] \xi^{1/2} \Xi_\beta^F(\xi) = 0 \; , \quad (3a)$$

$$\left[\frac{d^2}{d\eta^2} + \left[-\frac{m^2 - 1}{4\eta^2} + \frac{1 - \beta}{\eta} + \frac{1}{2}\epsilon + \frac{1}{4}F\eta \right] \right] \times \eta^{1/2} \Upsilon_\beta^F(\eta) = 0 \; . \quad (3b)$$

The total energy-normalized wave function, regular at $r = 0$, is then

$$\psi_{\epsilon n_1 m}^F = \psi_\beta^F(\xi, \eta, \phi) = \frac{e^{im\phi}}{\sqrt{2\pi}} \Xi_\beta^F(\xi) \Upsilon_\beta^F(\eta) \; . \quad (4)$$

The factors $\xi^{1/2}$ and $\eta^{1/2}$ in Eqs. (3a) and (3b) remove first derivatives. We will frequently omit the indices m and ϵ, which remain good quantum numbers. All quantities considered here are continuous functions of the energy.

The *separation parameters* $\beta \equiv \beta_1$ and $1 - \beta \equiv \beta_2$ appear in Eqs. (3a) and (3b) as fractional Coulomb charges. In this sense—and for fixed m, F, ϵ—β determines the partition of nodes between the functions $\Xi_\beta^F(\xi)$ and $\Upsilon_\beta^F(\eta)$, which extend in the up-field (large ξ) and down-field (large η) directions, respectively. The quantity

$$A_z \equiv \beta_1 - \beta_2 = 2\beta - 1 = (n_1 - n_2)/n$$

represents in fact the eigenvalue of the z component

of the Runge-Lenz vector,

$$\vec{A} = \hat{r} - \tfrac{1}{2}(\vec{p} \times \vec{L} - \vec{L} \times \vec{p}) + O(F) \; ,$$

operating on the quasibound states. At $F=0$, the conservation of both $\vec{A}$ and the angular momentum $\vec{L}$ follows from the $SU(2) \times SU(2)$ symmetry of a pure Coulomb field.[13,16] Classically, A_z represents the constant direction of the major axis of a Keplerian orbit with given eccentricity or angular momentum. In wave mechanics, of course, bound orbits are quantized. In the presence of a Stark field, quantization occurs only in the motion in ξ [see Eq. (25) of I]:

$$\int_{\xi_1}^{\xi_2} \left[-\frac{m^2}{4\xi'^2} + \frac{\beta_1}{\xi'} + \tfrac{1}{2}\epsilon - \tfrac{1}{4}F\xi' \right]^{1/2} d\xi'$$

$$= \pi(n_1 + \tfrac{1}{2}) \; . \quad (5)$$

Note that $\Xi_\beta^F(\xi)$ is bound at *all* ϵ for $F \neq 0$, owing to the confining potential $+Fz$, whereas $\Upsilon_\beta^F(\eta)$ can tunnel to $\eta \to \infty$ even for $\epsilon < 0$ and thus belongs to a continuous spectrum. For fixed F and m and for a given number of nodes $n_1 = 0, 1, 2, \ldots$ in ξ, the real eigenvalue

$$\beta(\epsilon, F; n_1, m) \equiv \beta_{\epsilon n_1 m}^F$$

defined by Eq. (3) is a monotonically decreasing function of ϵ (see Ref. 10, Fig. 2); at all ϵ there is a one-to-one correspondence between n_1 eigenchannels and the discrete eigenvalues $\beta_{\epsilon n_1 m}^F$. We will use the channel labels n_1 and β interchangeably and sometimes write simply β for $\beta_{\epsilon n_1 m}^F$. The orthonormal set of parabolic eigenfunctions $\Xi_\beta^F(\xi)$ (at fixed ϵ) plays a role in Eq. (4) equivalent to that of the associated Legendre polynomials $P_{lm}(\cos\theta)$ in the spherical eigenfunctions of H.

A second eigenchannel parameter is $N_{\epsilon n_1 m}^F \equiv N_\beta^F > 0$, the *energy-normalization amplitude* of $\psi_{\epsilon n_1 m}^F \equiv \psi_\beta^F$, which is fixed at $\eta \to \infty$ such that

$$\int \psi_{\epsilon' n_1 m}^F \psi_{\epsilon n_1 m}^F d\tau = \delta(\epsilon' - \epsilon) \; .$$

[The notation here differs from that of paper I (see Ref. 10), which defined $N_{\epsilon n_1 m}^F$ as an *intensity*.] The squared amplitude $(N_{\epsilon \beta m}^F)^2$ represents the density of states at $\xi \sim \eta \sim 0$ in the n_1 channel; N_β^F itself constitutes the energy-dependent factor in ψ_β^F near the core:

$$\psi_\beta^F(\xi \sim 0, \eta \sim 0)$$

$$= N_{\epsilon \beta m}^F \{ e^{im\phi} (2\pi)^{-1/2} (\xi\eta)^{m/2} [1 + O(r)] \} \; . \quad (6)$$

Note that the bracketed function in Eq. (6), $\psi_{\epsilon \beta m}^F / N_{\epsilon \beta m}^F$ is essentially energy-independent, to $O(r)$. Its behavior at small r is determined instead by β and m; its dependence on ϵ is relatively insignificant, owing to the large kinetic energy at small r. When $\epsilon < 0$, the important effects of the barrier formed at large η by the Coulomb and Stark potentials are represented then by exponentially small values of $N_{\epsilon \beta m}^F$ except for sharp peaks at quasibound Stark-energy levels (see Sec. III and Appendix A). These levels quickly broaden out at $\epsilon \gtrsim \epsilon_c = -2\sqrt{\beta_2 F}$, where the critical energy ϵ_c marks the top of the η barrier in an n_1 channel.

In each n_1 channel with $m \neq 0$ and $\epsilon > 0$, $N_{\epsilon \beta m}^F$ peaks as a function of the energy at $\beta_1 \approx \beta_2 \approx \tfrac{1}{2}$, since $|\psi|^2$ then tends to be repelled from the z axis by centrifugal forces. In general, according to I,[20] we have

$$|N_{\epsilon \beta m}^F|^2 \propto (\beta_1 \beta_2)^m, \quad 0 < \beta_1 = 1 - \beta_2 < 1 \; . \quad (7)$$

If $m=0$, on the other hand, $N_{\epsilon \beta 0}^F$ is not strongly sensitive to the direction and $|\psi|^2$ may thus be appreciable along the z axis, i.e., at $\beta_{\epsilon n_1 0}^F \approx 1$ (or 0). If either $\beta_1 = \beta < 0$ or $\beta_2 < 0$ $(\beta > 1)$, however, the Coulomb barrier formed in ξ or η renders $N_{\epsilon \beta m}^F$ exponentially small. In fact, $N_{\epsilon \beta 0}^F$ changes dramatically whenever $\beta_2 = 1 - \beta_{\epsilon n_1 0}^F$ passes through zero in the range $\epsilon = \tfrac{1}{2} k^2 \gtrsim 0$: For $\beta_2 \approx 0$, $N_{\epsilon \beta 0}^F \propto (1 + e^{-\pi \beta_2 / k})^{-1/2}$ rises very abruptly[10] from $\sim e^{-|\pi\beta_2/2k|}$ to about $1/n_1$ in a given n_1 channel. [This effect is smoothed out for $m \neq 0$, since $(N_\beta^F)^2$ is already small according to Eq. (7).] In the following, we shall ignore those channels below threshold with $\beta_2 < 0$, since then

$$(N_\beta^F)^2 < \exp(-|2\epsilon|^{3/2}/3F)$$

is always negligible.

The energies $\epsilon_{n_1}^F$ at which $\beta_{\epsilon n_1 0}^F \approx 1$ correspond then to the following joint condition: (a) concentration of $\psi_{\epsilon n_1 0}^F$ along the positive z axis with n_1 nodes, and (b) maximal amplitude of $\psi_{\epsilon n_1 0}^F$ at $r = O$ (1 a.u.). The energies $\epsilon_{n_1}^F$ mark the resonance peaks observed at $\epsilon \gtrsim 0$ for $m(\text{final}) = 0$ in the total photoionization cross section, which favors excitation along the z axis.

B. Coordinate transformation

The transformation between regular eigenfunctions in spherical and parabolic coordinate bases

emerges when we first consider the pure Coulomb potential. At zero field the nth level of the discrete Rydberg spectrum $(\epsilon = -\frac{1}{2}n^{-2})$ has n^2 degenerate eigenfunctions. For each $|m| = 0,1,\ldots,n-1$ of a particular level, one can construct a complete set of $n - |m|$ orthogonal eigenfunctions in either spherical or parabolic coordinates. (For $\epsilon > 0$ instead, these eigenfunctions are denumerably infinite in l or continuous in β.) The discrete eigenfunctions are energy normalized, in the sense that

$$\int \psi_{\epsilon'}\psi_\epsilon d\tau = \delta_{n'n}\frac{dn}{d\epsilon} = n^3\delta_{n'n} . \tag{8}$$

Any one of the parabolic functions can be expanded in the set of spherical functions,[21] or vice versa:

$$\psi_{\epsilon\beta m}^{F=0} = \sum_{l=m}^{\infty} U_{\beta l}^{\epsilon m}\psi_{\epsilon l m} , \tag{9}$$

where the expansion coefficients $U_{\beta l}^{\epsilon m}$ are limited to $l \le n-1$ when $\epsilon < 0$. When $\psi_{\epsilon\beta m}^{F=0}$ and $\psi_{\epsilon l m}$ are normalized as in (8), the transformation matrix $U_{\beta l}^{\epsilon m} = \langle \epsilon\beta m \mid \epsilon l m \rangle$ is orthogonal for fixed ϵ and m, i.e., $\widetilde{U}_{l\beta} = (U^{-1})_{l\beta}$:

$$\sum_{n_1} \widetilde{U}_{l'\beta}^{\epsilon m'} U_{\beta l}^{\epsilon m} = \delta_{l'l}\delta_{m'm} , \tag{10a}$$

$$\sum_{l} U_{\beta'l}^{\epsilon m'} \widetilde{U}_{l\beta}^{\epsilon m} = \delta_{\beta'\beta}\delta_{m'm} . \tag{10b}$$

The sum over n_1 in Eq. (10a) actually stands for a sum over the eigenvalues

$$\beta_{\epsilon n_1 m}^{F=0} = (n_1 + \frac{1}{2} + \frac{1}{2}m)/n .$$

In fact, $U_{\beta l}^{\epsilon m}$ is Wigner coefficient which couples spinor eigenfunctions of $\frac{1}{2}(\vec{L}\pm\vec{A})$,[16]

$$U_{\beta l}^{\epsilon m} = \langle lm \mid j\mu_+, j\mu_- \rangle , \tag{11}$$

where $j = \frac{1}{2}(\nu-1)$, $\mu_\pm = \frac{1}{2}(m \pm \nu A_z)$, $\nu = (-2\epsilon)^{-1/2}$, and $A_z = 2\beta - 1$.

Equation (11) has been presented here for zero field and $\epsilon < 0$. Formal extension to continuum states and nonzero field implies that j and $\mu_\pm$ are no longer rational, or even real, for $\epsilon \ge 0$. The formula extends nevertheless to such values by analytic continuation,[13] but it must be complemented by factors that reflect the proper normalization of the wave functions.

In the presence of a finite Stark field, $\psi_{\epsilon\beta m}^F$ is a continuum function at $\epsilon = -\frac{1}{2}\nu^{-2} < 0$ as well as at $\epsilon = \frac{1}{2}k^2 \ge 0$, energy normalized according to

$$\int \psi_{\epsilon'}\psi_\epsilon d\tau = \delta(\epsilon' - \epsilon) \tag{8'}$$

as in Sec. II A. The energy normalization depends on the wave function's behavior in the Coulomb and Stark potentials at $r \to \infty$. However, the coordinate transformation is of interest at *small* r, where the Stark field is negligible, because the overlap between $\psi_{\epsilon\beta m}^F$ and the localized initial state ψ_i in the transition dipole $\langle \psi_\beta^F \mid r \mid \psi_i \rangle$ is appreciable only for $r \lesssim 0 - 10$ a.u. We should like, therefore, to separate the dependence of the expansion coefficients $U_{\beta l}^{\epsilon m}$ from the influence of long-range fields and of details of the energy normalization. Accordingly, we explicitly factor out the energy-normalization amplitude $N_{\epsilon\beta m}^F$ from $\psi_{\epsilon\beta m}^F$, as in Eq. (6). Similarly, we factor out the normalization amplitude $N_{\epsilon l}$ from the zero-field spherical function $\psi_{\epsilon l m}$:

$$\psi_l(r \sim 0) = N_{\epsilon l}\{e^{im\phi}(2\pi)^{-1/2}P_{lm}(\cos\theta)r^l[1+O(r)]\} , \tag{12}$$

where[15,18]

$$N_{\epsilon l} = \frac{2^{l+1}}{(2l+1)!}\left[\prod_{p=0}^{l}(1+2\epsilon p^2)\right]^{1/2}\begin{cases}1, & \epsilon = -\frac{1}{2}\nu^{-2} < 0 \\ (1-e^{-2\pi/k})^{-1/2}, & \epsilon = \frac{1}{2}k^2 > 0 .\end{cases} \tag{13}$$

Note, however, that for $\epsilon < 0$ (discrete spectrum) and $\epsilon > 0$ (continuum) the normalizations (8) and (8') for $\psi_{\epsilon l m}$ differ by

$$\delta(\epsilon' - \epsilon)\nu^{-3} = \delta(\nu' - \nu) .$$

We now consider the wave functions $\psi_{\epsilon\beta m}^F / N_{\epsilon\beta m}^F$ and $\psi_{\epsilon l m}/N_{\epsilon l}$ [in braces in Eqs. (6) and (12)], which are normalized independently of energy at the origin. (The role of energy-independent normalization

has been described in Ref. 18.) These functions are completely characterized in the Coulomb potential at small r by their values of $\beta_{\epsilon n_1 m}^F$ and l, respectively, along with ϵ and m. The fact that $\beta_{\epsilon n_1 m}^F$ is determined by a boundary condition at large ξ is irrelevant to the transformation at small r, i.e.,

$$\psi_{\epsilon\beta m}^F / N_{\epsilon\beta m}^F = \psi_{\epsilon\beta m}^{F=0} / N_{\epsilon\beta m}^{F=0}, \quad r \ll F^{-1/2} . \tag{14}$$

We therefore write an expansion analogous to (9),

$$\psi^F_{\epsilon\beta m}/N^F_{\epsilon\beta m} = \sum_{l=m}^{\infty} a^{\epsilon m}_{\beta l}(\psi_{\epsilon lm}/N_{\epsilon l}), \quad r \ll F^{-1/2} .$$

(15)

The coefficients $a^{\epsilon m}_{\beta l}$ are now *free* from the effects of the Stark and Coulomb potentials at large r (except for the implicit dependence on F through the eigenvalues β), which are instead embodied in the amplitudes $N^F_{\epsilon\beta m}$ and $N_{\epsilon l}$. By rewriting Eq. (15) in the form

$$\psi^F_{\epsilon\beta m} = \sum_{l=m}^{\infty} (a^{\epsilon m}_{\beta l} N^F_{\epsilon\beta m}/N_{\epsilon l})\psi_{\epsilon lm} \equiv \sum_{l} U_{\beta l}\psi_{\epsilon lm} ,$$

(16a)

we explicitly *extend the transformation* (9) to nonzero F in the region where F is still negligible. We also formally specify the transformation inverse to Eq. (16),

$$\psi_{\epsilon lm} = \sum_{\beta} (U^{-1})_{l\beta}\psi^F_{\epsilon\beta m} ,$$

(16b)

but will never actually need to calculate $(U^{-1})_{l\beta}$.

The coefficients $a^{\epsilon m}_{\beta l}$ of Eq. (16a) embody the purely geometrical aspects of the coordinate transformation, which are represented by the Wigner coefficient (11) in the special case $F=0$, $\epsilon < 0$. In general, $a^{\epsilon m}_{\beta l}$ remains real, even though the parameters ν and $\mu_\pm$ of Eq. (11) become imaginary. These coefficients,

$$a^{\epsilon m}_{\beta l} = \frac{(-1)^m\sqrt{4l+2}\,m\,!^2}{(2l+1)!![(l+m)!(l-m)!]^{1/2}} \sum_{k=0}^{l-m}(-1)^k \begin{bmatrix} l-m \\ k \end{bmatrix} \begin{bmatrix} l+m \\ l-k \end{bmatrix} \frac{\Gamma(n_1+1)\nu^{m-l}\Gamma(n_2+1)}{\Gamma(n_1+1-k)\Gamma(n_2+1-l+m+k)} ,$$

(17)

where $n_i \equiv \beta_i\nu + \frac{1}{2} + \frac{1}{2}m$ $(i=1,2)$, are polynomials of order $l-m$ in $A_z = 2\beta - 1$, just as the associated Legendre polynomials are of order $l-m$ in $\cos\theta$ and $\sin\theta$; the first few coefficients are given in Table I. [The factors that multiply the Wigner coefficient in Eq. (13) of Ref. 13 are represented in our Eq. (16) by the ratio $N_{\epsilon l}/N^{F=0}_{\epsilon\beta m}$.]

The transformation between parabolic and spherical bases, Eqs. (16a) and (16b), is appropriate to the pure Coulomb region $r \ll F^{-1/2}$ a.u., for any β or l.

In the parabolic region, however, the Schrödinger equation is not separable in spherical coordinates. Here the parabolic eigenfunctions $\psi^F_{\epsilon\beta m}$ of Eq. (1) cannot be expanded into the set of spherical functions $\{\psi_{\epsilon lm}\}$, which satisfy a Schrödinger equation for a different potential (i.e., $F=0$) at the same ϵ. Therefore, the transformation matrix $U_{\beta l}$ is *non*orthogonal at fixed ϵ, except for the special case $F=0$, where

$$\sum_{\beta} \widetilde{U}_{l'\beta} U_{\beta l} \xrightarrow[F\to 0]{} \delta_{l'l} \begin{cases} 1, & \epsilon \geq 0 \\ \delta(\nu'-\nu)\delta_{\nu n}, & \epsilon = -\frac{1}{2}\nu^2 \ (n=1,2,\dots) . \end{cases}$$

(18)

The $\epsilon < 0$ form of Eq. (18) follows from the different normalization conditions (8) and (8') for the discrete and continuous eigenfunctions, as noted above.

C. Photoabsorption cross sections in H

The cross section for single-photon excitation of the ground state $|0\rangle$ of H is given by an incoherent sum over all independent continuum channels,

$$\sigma^F(\epsilon) = (4\pi^2\alpha)\hbar\omega \sum_{n_1=0}^{\infty} |\langle \psi^F_{\epsilon\beta m} | r_m | 0 \rangle|^2 ,$$

(19)

where $\alpha = 1/137$, the photon energy is $\hbar\omega = \epsilon + \frac{1}{2}$ a.u., and $r_m = r\cos\theta$ for π polarization and

$$r_m = r\sin\theta e^{\pm i\phi}/\sqrt{2}$$

for $\sigma^\pm$ polarization. [Note that $\sigma^F(\epsilon)/2\pi^2\alpha$ equals the density of oscillator strengths $(df/d\epsilon)_F$.] In or-

der to express Eq. (19) in terms of ordinary atomic parameters, we expand the parabolic function $\psi^F_{\epsilon\beta m}$ into spherical functions $\psi_{\epsilon lm}$ at small r, where it overlaps $|0\rangle$. Insertion of the expansion (16a) into the dipole integral in Eq. (19) yields

TABLE I. Expansion coefficients $a^{\epsilon m}_{\beta l}$ defined by Eqs. (14)–(17); $A_z = \beta_1 - \beta_2 = 2\beta^F_{\epsilon n_1 m} - 1$.

$l=0$		1	2
$m=0$	$\sqrt{2}$	$-(\frac{2}{3})^{1/2}A_z$	$+(\frac{1}{40})^{1/2}[A_z^2 - \frac{1}{3}(1+2\epsilon)]$
1	0	$-(\frac{4}{3})^{1/2}$	$+(\frac{1}{15})^{1/2}A_z$
2	0	0	$+(\frac{16}{15})^{1/2}$

$$\langle \psi^F_{\epsilon \beta m} \mid r_m \mid 0 \rangle = \sum_{l=m}^{\infty} U_{\beta l} \langle \psi_{\epsilon l m} \mid r_m \mid 0 \rangle \;, \quad (20)$$

$$U_{\beta l} \equiv U^{\epsilon m}_{\beta l} = a^{\epsilon m}_{\beta l} (N^F_\beta / N_l) \;, \quad (21)$$

with $U_{\beta l}$ from Eq. (16a). The dipole selection rule $\Delta l = \pm 1$ implies that only the $l = 1$ term survives in Eq. (20), since $l = 0$ initially. The cross section (19) thus reduces to

$$\sigma^F(\epsilon) = (4\pi^2 \alpha \hbar \omega \mid \langle \psi_{\epsilon l m} \mid r_m \mid 0 \rangle \mid^2) \sum_{n_1=0}^{\infty} (U_{\beta 1})^2 \;.$$

$$(22)$$

This result was obtained in slightly different form in Sec. I B of paper I. The bracketed expression in Eq. (22) is simply the *zero-field photoabsorption cross section*, $\sigma^{F=0}(\epsilon)$, for a hydrogenic $s \rightarrow p$ transition, which extrapolates smoothly to $\epsilon < 0$ by the normalization (8) of $\psi_{\epsilon l m}$. Thus, $\sigma^{F=0}(\epsilon)$ represents the average oscillator-strength density at $\epsilon < 0$ and varies only slowly within 0.1 eV of threshold. The fact that $\sigma^{F=0}(\epsilon)$ can be explicitly factored out of $\sigma^F(\epsilon)$—even when there is a finite Stark field—is a major feature of the present theory and will apply in a similar way to the alkali cross sections.

The sum of squared expansion coefficients in Eq. (22) appears as an energy-dependent *modulating factor*, $H^F(\epsilon)$, which multiplies $\sigma^{F=0}(\epsilon)$. The same values of l ($l = 1$) and m (0 or 1) appear twice in each term $U^{\epsilon m}_{\beta l} U^{\epsilon m}_{\beta l}$, since the squared dipole enters into the single-photon cross section (19). However, two alternative values (l,l') occur generally in two-step photoionizaton for the final state ψ_f. *Interference* terms will then arise between different l channels in ψ_f. Therefore, we define a more general modulating factor $H^F_{l'l}$ as a matrix element (in an infinite $l \times l$ space) of the squared transformation matrix (21):

$$H^F_{l'l} \equiv \langle l'm' \mid H^F \mid lm \rangle \equiv \delta_{m'm} \sum_{\beta} U^{\epsilon m'}_{\beta l'} U^{\epsilon m}_{\beta l} \;.$$

$$(23a)$$

Cross terms with $m' \neq m$ do not appear in Eq. (23a) since m is a good quantum number. We will often use matrix notation, writing

$$H^F = \tilde{U} U \;, \quad (23b)$$

with the indices $l'l$ and the sum $\sum_{\beta}$ understood. Note that the matrix $H^F_{l'l}$ is symmetric in $l' \leftrightarrow l$. In the limit $F \rightarrow 0$, $H^F_{l'l}$ becomes diagonal because Eq. (23a) reduces to the orthonormality condition (18), and the total cross section (22) (with $l' = l = 1$) reduces to its proper analytical form for hydrogen,

$$\sigma^F(\epsilon) \xrightarrow[F \rightarrow 0]{} 2\pi^2 \alpha \begin{cases} \left[\dfrac{df}{d\epsilon} \right]_{F=0}, & \epsilon \geq 0 \\[2ex] f_n \delta(\epsilon + \tfrac{1}{2} n^{-2}), & \epsilon < 0 \;, \end{cases} \quad (24)$$

where f_n is the oscillator strength for a $1s \rightarrow np$ transition.

It is important that $H^F(\epsilon)$ depends only on the *final*-state hydrogen-Stark wave functions $\psi^F_{\epsilon \beta m}$. The identity of the initial state and even the details of the transition itself are contained entirely in $\sigma^{F=0}(\epsilon)$, except for the specification of the final-state angular quantum numbers l and m. The effects of the Stark field are contained instead in $H^F(\epsilon)$, to the extent that $H^F_{l'l}$ differs from $\delta_{l'l}$, Eq. (18).

An alternative and, for our purposes, more fundamental derivation of $\sigma^F(\epsilon)$ follows from first considering the photoabsorption process proper, represented by $\langle \psi_f \mid r_m \mid 0 \rangle$. Excitation of the ground state $\mid 0 \rangle$ leads to the excited state $\mid \psi_f \rangle$ in the limited region of their overlap, $r \ll F^{-1/2}$ a.u. In this region the final state is equal to $\psi_{\epsilon, l=1, m}$, to within normalization. The evolution of $\psi_{\epsilon l m}$ to continuum behavior at large distances is then represented by its expansion (16b) into parabolic functions. However, the superposition (16b) is no longer normalized to $\delta_{l'l} \delta(\epsilon' - \epsilon)$, nor is the set $\{ \psi_{\epsilon l m} \}$, in general, orthonormalized, because $U_{\beta l}$ is not a unitary transformation since $[(H^F)^{-1}]_{l'l}$ replaces $\delta_{l'l}$ in the overlap matrix

$$\langle \psi_{\epsilon' l' m'} \mid \psi_{\epsilon l m} \rangle = \sum_{\beta} (U^{-1})_{l'\beta} (\tilde{U}^{-1})_{\beta l} \delta_{m'm} \delta(\epsilon' - \epsilon)$$

$$= [(\tilde{U} U)^{-1}]_{l'l} \delta_{m'm} \delta(\epsilon - \epsilon)$$

$$= [(H^F)^{-1}]_{l'l} \delta_{m'm} \delta(\epsilon' - \epsilon) \;. \quad (25)$$

Orthonormalization of the states $\{ \psi_{\epsilon l m} \}$ by the matrix $\langle \psi' \mid \psi \rangle^{-1/2}$ now leads to the cross section

$$\sigma^F(\epsilon) = 4\pi^2 \alpha \hbar \omega \langle 0 \mid r_m \mid \psi_{\epsilon l' m} \rangle [\langle \psi' \mid \psi \rangle^{-1}]_{l'l}$$

$$\times \langle \psi_{\epsilon l m} \mid r_m \mid 0 \rangle, \quad l' = l = 1 \quad (26)$$

which is identical to the expression (22) with

$$D^F_{l'l} \equiv [\langle \psi' \mid \psi \rangle^{-1}]_{l'l} = H^F_{l'l} \;. \quad (27)$$

Note that the normalization factor $\delta(\epsilon' - \epsilon)$ in Eq. (25) has been absorbed into the dipole matrix elements in Eq. (26), so the inversion in Eq. (27) is restricted to the matrix of coefficients $[(H^F)^{-1}]_{l'l}$.
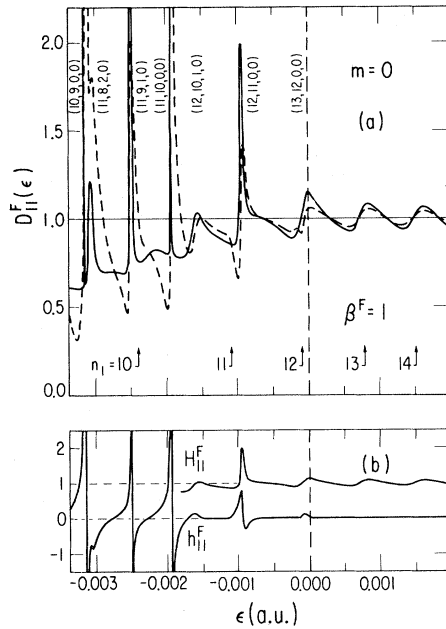
FIG. 1. (a) DOS matrix element $D_{l'l}^F$ for $F=77$ kV/cm, $m=0$, $l'=l=1$, near the ionization threshold ($\epsilon=0$). —— H_{11}^F, hydrogen; ---- D_{11}^F, Na [Eq. (58)]. Quasidiscrete Stark levels labeled by (n,n_1,n_2,m). Arrows numbered by n_1 mark $\beta_{\epsilon n_1 0}^F=1$, i.e., resonances at $\epsilon=\epsilon_{n_1}^F$. (b) H_{11}^F and h_{11}^F, Eqs. (23) and (55), for $m=0$, same F. Note anomalous dispersion in h_{11}^F at Stark resonances.
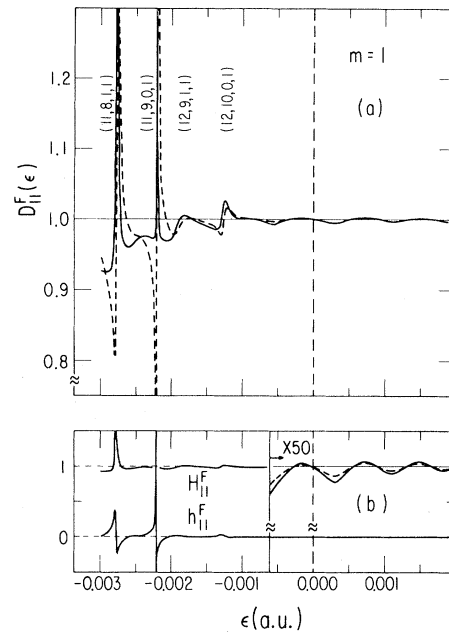

FIG. 2. Matrix elements as in Fig. 1, but with $m=1$ and expanded vertical scale: (a) D_{11}^F for H and Na, (b) H_{11}^F and h_{11}^F. Note Stark levels and detail of small threshold modulations in H_{11}^F.

The factorized form of $\sigma^F(\epsilon)$ therefore has a direct interpretation in terms of the separate physical effects of (a) photoabsorption and (b) ionization in the long-range Coulomb-Stark potential.

Figure 1(a) (solid line) shows $H_{11}^F(\epsilon)$ for

$$F=1.5\times10^{-5} \text{ a.u.} =77 \text{ kV/cm} ,$$

final $m=0$ (π polarization), and $\epsilon\sim0$. The parameters $\beta_{\epsilon n_1 m}^F$ and N_β^F for Fig. 1 (and all other figures herein) were calculated by the WKB procedures described in paper I. We note here a few general features of $H^F(\epsilon)$.

(1) The sharp symmetric peaks, which correspond to the highly excited, quasidiscrete Stark states, broaden out and disappear above $\epsilon\approx-0.001$ a.u.

(2) Regular modulations set in at $\epsilon\approx-0.002$ a.u., persist *beyond* threshold, and peak at the resonance energies $\epsilon_{n_1}^F$ marked by the arrows and their values of n_1 in Fig. 1(a). These features overlap the sharp peaks in a small region below threshold.

(3) At $\epsilon\geq0$, H^F ranges equally above and below $H^F=1$. Thus, the presence of a Stark field induces an *oscillatory* modulation of the zero-field cross sec-

tion, so that the oscillator-strength density is (at least approximately) conserved *on the average* above threshold. The spacing and depth of the modulations grow with increasing F and reduce instead to $H^F(\epsilon)=$const$=1$ as $F\rightarrow0$.

(4) The background at $\epsilon<0$ drops to zero at the classical ionization energy $\epsilon_{\text{ion}}=-\sqrt{4F}$ and rises to unity at $\epsilon>0$. The envelope or depth of modulations, $2|H^F-1|$, decreases at $\epsilon>0$ roughly as

$$4\exp[-3(\epsilon-\epsilon_{\text{ion}})/|\epsilon_{\text{ion}}|]$$

$$\approx0.20\exp(-3\epsilon/|\epsilon_{\text{ion}}|) .$$

Figure 2(a) (solid) shows $H_{11}^F(\epsilon)$ for $|m|=1$ ($\sigma^\pm$ polarization) and $F=77$ kV/cm, with the vertical scale expanded [see also Fig. 2(b)]. Above threshold, H_{11}^F-1 is only a fraction of a percent; below threshold, of course, one still observes sharp peaks at the Stark levels.

D. Photoabsorption from an excited state

The extension of the cross-section formula (22) to include two-photon transitions through an excited intermediate state is straightforward. Here we consider the following case.

(1) The first photon excites the ground state to an np state, ψ_i, saturated by a laser.

(2) ψ_i is described by a superposition of $l m_l s m_s$ basis states (to be ls coupled in Sec. IV to a specific $j m_j$ state, $j = \frac{1}{2}$ or $\frac{3}{2}$).

(3) ψ_i is localized within a region where the Stark field is still negligible; this requires $n \ll F^{-1/4}$ (see Sec. I B of paper I).

In hydrogen, one should also take into account the linear Stark splitting of the nth level, $\Delta\epsilon = \frac{3}{2} n^2 F(2\beta - 1)$. We forego this complication, however, because of our primary concern with applications to nonhydrogenic atoms, whose linear Stark shift is zero and whose quadratic Stark shift is negligible.

The total cross section (19) for absorption of the second (ionizing) photon is therefore given by Eq. (22), with $|\psi_i\rangle$ in place of $|0\rangle$. Once more, Eq. (14) holds insofar as ψ_i and $\psi_{\epsilon\beta m}^F$ overlap appreciably only where $Fz \ll 1/r$. Now the dipole integral (20) contains both $p \rightarrow d$ and $p \rightarrow s$ transitions if

m(final) $\equiv m_f = 0$, but only $p \rightarrow d$ if $m_f = 1$ or 2. The hydrogenic photoionization cross section thus becomes

$$\sigma^F(\epsilon) = \sigma_{22}^{F=0}(\epsilon) H_{22}^F(\epsilon) + 2\sigma_{20}^{F=0}(\epsilon) H_{20}^F(\epsilon)$$
$$+ \sigma_{00}^{F=0}(\epsilon) H_{00}^F(\epsilon) , \qquad (28)$$

where the modulating factor $H_{l'l}^F$ is defined by Eqs. (23a) and (21). The presence of the cross term in Eq. (28) requires us to define

$$\sigma_{l'l}^{F=0}(\epsilon)$$

$$= (4\pi^2\alpha) \hbar\omega \langle \psi_i | r_m | \psi_{\epsilon l'm} \rangle \langle \psi_{\epsilon lm} | r_m | \psi_i \rangle ; \qquad (29)$$

we will henceforth omit the superscript $F=0$ of σ. [Note that the angular brackets in Eq. (29) indicate both radial and angular integration.] The zero-field total cross section, $\sum_l \sigma_{ll} = \sigma_{22} + \sigma_{00}$, may be factored out of Eq. (28) as in Eq. (22) by writing

$$\sigma^F(\epsilon) = (\sigma_{22} + \sigma_{00}) \left[\frac{\sigma_{22} H_{22}^F + 2\sigma_{20} H_{20}^F + \sigma_{00} H_{00}^F}{\sigma_{22} + \sigma_{00}} \right] . \qquad (30)$$

The expression in parentheses in Eq. (30), $\sigma^F/(\sigma_{22} + \sigma_{00})$, represents the modulation of $(\sigma_{22} + \sigma_{00})$. The interference term between $l = 2$ and $l = 0$ channels, $2\sigma_{20} H_{20}^F$, may be of either sign, depending on the angular integrals in Eq. (29). In the limit $F \rightarrow 0$ this term vanishes owing to Eq. (18), and Eq. (30) reduces to the zero-field analog of Eq. (24) for two l channels.

The cross section (28) generalizes Eq. (26) since photoexcitation to final s and d states in the region
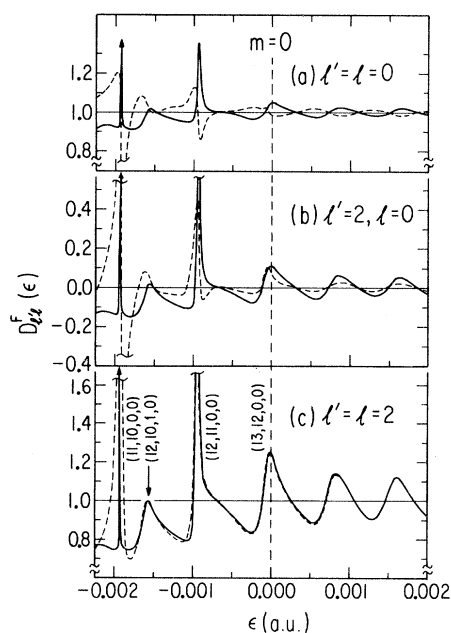

FIG. 3. DOS matrix elements $D_{l'l}^F$ for H and Na as in Fig. 1(a), $m = 0$: (a) D_{00}^F, (b) $D_{20}^F = D_{02}^F$, (c) D_{22}^F.
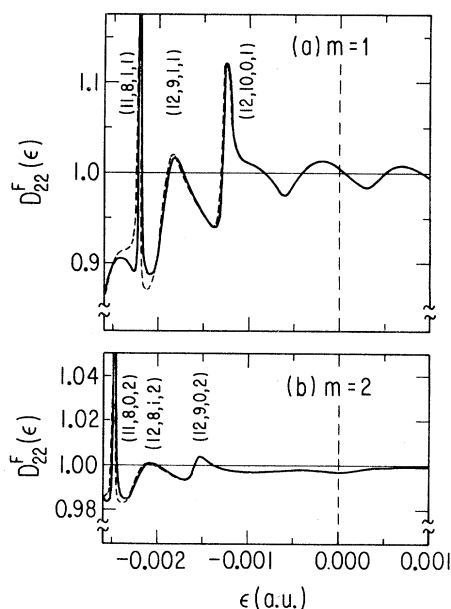
FIG. 4. D_{22}^F for H and Na as in Fig. 3(c), but with (a) $m = 1$, (b) $m = 2$. D_{22}^F and H_{22}^F almost coincide since $\mu_2 \sim 0$.

TABLE II. Hydrogenic cross sections for photoionization from an intermediate np state, Eq. (28); see Eqs. (21)—(24); $\sum_\beta \equiv \sum_{n_1=0}^{\infty}$, $\beta^F \equiv \beta^F_{\epsilon n_1 m}$.

$$G_1(\epsilon) \equiv (4\pi^2\alpha)[2^{15}3^8(1+18\epsilon)^{-7}] \begin{cases} \left[\dfrac{\nu-3}{\nu+3}\right]^{2n}, & \epsilon = -\tfrac{1}{2}\nu^{-2} < 0 \\[2ex] e^{-(4/k)\tan^{-1}3k}(1-e^{-2\pi/k})^{-1}, & \epsilon = \tfrac{1}{2}k^2 \geq 0 \end{cases}$$

$$G_2(\epsilon) \equiv G_1(\epsilon)/240$$

Polarizations	$m_i \to m_f$	$\sigma^F(\epsilon)/4\pi^2\alpha\hbar\omega$	$\sigma^F(\epsilon),\ \lvert\psi_i\rangle = \lvert n=3, l=1, m=0 \text{ or } 1\rangle$
$\pi\pi$	$0\to0$	$\frac{4}{15}(R_{n1}^{\epsilon2})^2 H_{22}^F$	$G_1(\epsilon)\sum_\beta (N_\beta^F)^2\frac{1}{64}[(2\beta^F-1)^2-\frac{2}{9}]^2$
	(H^F for $m=0$)	$+\dfrac{4}{3\sqrt5}(R_{n1}^{\epsilon2}R_{n1}^{\epsilon0})H_{20}^F+\frac{1}{3}(R_{n1}^{\epsilon0})^2 H_{00}^F$	$\underset{F\to0}{\to} G_2(\epsilon)(\frac{41}{54}+\frac{80}{9}\epsilon+14\epsilon^2)$
$\sigma^+\sigma^-$ or $\sigma^-\sigma^+$	$1\to1$	$\frac{1}{15}(R_{n1}^{\epsilon2})^2 H_{22}^F$	$G_1(\epsilon)\sum_\beta (N_\beta^F)^2\frac{1}{256}[(2\beta^F-1)^2-(\frac{5}{9}+2\epsilon)]^2$
	(H^F for $m=0$)	$-\dfrac{2}{3\sqrt5}(R_{n1}^{\epsilon2}R_{n1}^{\epsilon0})H_{20}^F+\frac{1}{3}(R_{n1}^{\epsilon0})^2 H_{00}^F$	$\underset{F\to0}{\to} G_2(\epsilon)(\frac{7}{27}+\frac{35}{9}\epsilon+6\epsilon^2)$
$\pi\sigma^+$ or $\pi\sigma^-$	$0\to1$		$G_1(\epsilon)\sum_\beta (N_\beta^F)^2\frac{1}{32}(2\beta^F-1)^2$
$\sigma^+\pi$ or $\sigma^-\pi$	$1\to1$	$\frac{1}{5}(R_{n1}^{\epsilon2})^2 H_{22}^F$	$\underset{F\to0}{\to} G_2(\epsilon)\frac{1}{2}(1+2\epsilon)(1+8\epsilon)$
	(H^F for $m=1$)		
$\sigma^+\sigma^+$ or $\sigma^-\sigma^-$	$1\to2$	$\frac{2}{5}(R_{n1}^{\epsilon2})^2 H_{22}^F$	$G_1(\epsilon)\sum_\beta (N_\beta^F)^2 \underset{F\to0}{\to} G_2(\epsilon)(1+2\epsilon)(1+8\epsilon)$
	(H^F for $m=2$)		

$r \ll F^{-1/2}$ requires us to keep all four pairs of spherically symmetric wave functions $\lvert\psi_{l'}\rangle\langle\psi_l\rvert$, as in Eqs. (28) and (29). Renormalization by the DOS matrix (27) leads once more to Eq. (28) in the form

$$\sigma^F(\epsilon) = (4\pi^2\alpha)\hbar\omega \sum_{l'l} \langle\psi_i\lvert r_m\rvert\psi_{l'}\rangle[\langle\psi'\lvert\psi\rangle^{-1}]_{l'l}\langle\psi_l\lvert r_m\rvert\psi_i\rangle$$

$$= \sum_{l'l} [\langle\psi'\lvert\psi\rangle^{-1}]_{l'l}\sigma_{l'l}(\epsilon) = \text{Tr}[H^F\sigma(\epsilon)], \quad l',l = l_i\pm1 . \tag{31}$$

The three modulating factors $H_{00}^F(\epsilon)$, $H_{20}^F(\epsilon)$, and $H_{22}^F(\epsilon)$ are shown in Figs. 3(a)—3(c) (solid lines) for $m_f=0$ and $F=77$ kV/cm, while Figs. 4(a) and 4(b) show $H_{22}^F(\epsilon)$ for $m_f=1$ and 2 (and $F=77$ kV/cm). Note the qualitative similarity of all three curves in Fig. 3, especially the fact that they apparently oscillate in phase both above and below threshold. Also note that $\lvert H_{ll}^F-1\rvert$ increases with l at all ϵ; H_{20}^F is intermediate in magnitude between H_{00}^F and H_{22}^F; and $H_{22}^F(\epsilon)$ in Fig. 4 is much flatter above threshold for $m=1$ and 2, in analogy to Fig. 2(a) for $m=l=1$.

The nine possible polarization combinations of the two photons lead to only four distinct cross sections for the transition process $1s\to np\to\epsilon d+\epsilon s$: (a) $\pi\pi$, (b) $\sigma^+\sigma^-$, (c) $\pi\sigma^+$ (same as $\sigma^+\pi$), and (d) $\sigma^+\sigma^+$ (if we ignore ls coupling). The corresponding cross sections are listed in Table II in terms of the radial dipole matrix elements $R_{nl}^{\epsilon,l+1}$ and $R_{nl}^{\epsilon,l-1}$ ($l=1$) and of the values of the angular integrals. Also shown in Table II are the analytic expressions of the cross section (28) for a hydrogen $n=3$ intermediate state,[22] which are explicit functions of ϵ, $N_{\epsilon\beta m}^F$, and $A_z=2\beta-1$ (note that $\sigma_{00}=\sigma_{20}=0$ for $m_f=1$ and 2); the zero-field cross sections $\sigma(\epsilon)$ are analytical functions of ϵ alone.

The polarization dependence of the depth of modulations above threshold for ψ_i with $n=3$, $l=1$, $m=0$ or 1, is illustrated in Fig. 5, which shows all four $\sigma^F(\epsilon)$ on the same vertical scale (in a.u.; $F=77$ kV/cm). The dashed lines mark the cross sections for $F=0$ (see Table II). The qualitative features of these curves for two-photon excitation are the same as for single-photon excitation (cf. Figs. 1 and 2), but are enhanced here: The modulations are largest for $m_f=0$ and decrease for succes-
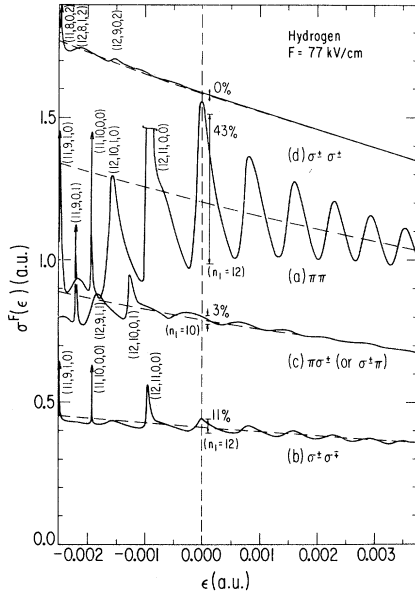
FIG. 5. Two-photon ionization cross sections for hydrogen $\sigma^F(\epsilon)$ for $F=77$ kV/cm: (a) $\pi\pi$ $(m=0\rightarrow m=0)$, (b) $\sigma^{\pm}\sigma^{\mp}$ $(m=1\rightarrow m=0)$, (c) $\pi\sigma^{\pm}$ or $\sigma^{\pm}\pi$ $(m=0\rightarrow m=1$ or $m=1\rightarrow m=1)$, (d) $\sigma^{\pm}\sigma^{\pm}$ $(m=1\rightarrow m=2)$; see Table II. Quasidiscrete Stark levels labeled by (n,n_1,n_2,m); depth of modulation and n_1 peak are shown at $\epsilon\approx 0$. ----, $\sigma^{F=0}(\epsilon)$.

sively larger values of m_f. This enhancement results from the larger value of l in the final state reached in the two-photon process. The size of l-m measures a spherical wave function's alignment along the z axis, maximal for $m=0$ and large l. This focusing translates into parabolic coordinates via the transformation coefficients $a_{\beta l}^{\epsilon m}$ (cf. Table I), which are most heavily weighted towards $A_z=\beta_1-\beta_2=\pm 1$ by their leading term A_z^{l-m}. The presence of an alkali-metal ion core will not alter this picture substantially.

III. PHOTOIONIZATION OF NONHYDROGENIC ATOMS

In Sec. II, we factored the photoionization cross section for hydrogen, Eqs. (19) and (28), or Eqs. (26)

and (31), into zero-field dipole matrix elements $\sigma_{l'l}(\epsilon)$ [Eq. (29)] and a density-of-states matrix $[\langle\psi'|\psi\rangle^{-1}]_{l'l}$ [Eqs. (27) and (23)]. This separation was effected via the coordinate transformation $a_{\beta l}^{\epsilon m}$ which is performed at $r\sim O$ (10 a.u.) and connects the spherical eigenfunctions $\psi_{\epsilon lm}$, appropriate at small r, to the parabolic eigenfunctions $\psi_{\epsilon\beta m}^F$, appropriate to the Coulomb-Stark potential at large r. The transformation is possible because both sets $\{\psi_{\epsilon lm}\}$ and $\{\psi_{\epsilon\beta m}\}$ are regular solutions of the *same* Schrödinger equation in the intermediate zone (2) characterized by a pure Coulomb potential.

In this section we apply the prescription of Sec. II to derive expressions for alkali cross sections $\sigma^F(\epsilon)$ analogous to Eqs. (26), (27), and (31) for H. We again utilize the transformation (16a) or (16b) in the Coulomb zone (2), but the presence of core effects necessitates an additional transformation for hydrogenic eigenfunctions *irregular* at $r=0$, which are defined through the Coulomb Green's function (Sec. III A). In the expressions for $\sigma^F(\epsilon)$ we then identify a generalized density-of-states matrix, $D_{l'l}^F\equiv[\langle\Psi'|\Psi\rangle^{-1}]_{l'l}$, which modulates the zero-field cross sections $\sigma_{l'l}$ of the alkalis (Sec. III B) and which contains all spectral information on the Stark effect, including asymmetric line shapes at $\epsilon<0$ and a series of modulations at $\epsilon\geq 0$ (Sec. III C). We shall characterize the asymmetry for the simplest case of D_{ll}^F by a Beutler-Fano parameter q, expressed analytically in terms of μ_l and of parameters of the hydrogenic-Stark spectrum. Differences between atoms appear *only* in their respective zero-field parameters $\sigma_{l'l}$ and μ_l, which we assume to be known from zero-field data.

We begin by considering an atom's final-state wave function in region (2) following photoabsorption. If the region $r\leq r_0$ is occupied by an alkali-metal ion core instead of a bare nucleus, each of the hydrogenic wave functions $\psi_{\epsilon lm}(\vec{r})$ acquires a radial phase shift $\delta_l=\pi\mu_l$ outside the core boundary r_0. The wave function $\Psi_{\epsilon lm}(\vec{r})$ of a nonhydrogenic atom is then written in terms of a radial base pair $[f_{\epsilon l}(r),g_{\epsilon_l}(r)]$ of regular and irregular Coulomb functions for the excited electron:

$$\Psi_{\epsilon lm}(\vec{r})=\cos\delta_l[f_{\epsilon l}(r)-\tan\delta_l g_{\epsilon l}(r)]Y_{lm}(\theta,\phi),\quad r>r_0 . \tag{32}$$

A factor representing the wave function for the core electrons is implicit in $\Psi_{\epsilon lm}$ but need not be spelled out, since we will never need to treat these electrons explicitly. The oscillations of $g_{\epsilon l}(r)$ in the range (2) lag 90° behind those of $f_{\epsilon l}(r)$. Both eigenfunctions are energy normalized, e.g., as WKB wave functions

$$f_{\epsilon l}(r)=[2/\pi k(r)]^{1/2}\sin\left[\int^r k(r')dr'+\tfrac{1}{4}\pi\right], \tag{33a}$$

$$g_{\epsilon l}(r) = -[2/\pi k(r)]^{1/2}\cos\left[\int^r k(r')dr' + \tfrac{1}{4}\pi\right], \quad r > r_0 \tag{33b}$$

with wave number

$$k(r) = [-(l+\tfrac{1}{2})^2/r^2 + 2/r + 2\epsilon]^{1/2}$$

and Wronskian $W_r(f_{\epsilon l}, g_{\epsilon l}) = 2/\pi$. [This energy normalization applies to $\epsilon \lesssim 0$ as well as to $\epsilon > 0$; cf. Eqs. (8) and (8').] For the total wave functions we

introduce the notation

$$f_l(\vec{r}) \equiv f_{\epsilon l}(r)Y_{lm}(\theta,\phi) = \psi_{\epsilon lm}(\vec{r}) , \tag{34a}$$

$$g_l(\vec{r}) \equiv g_{\epsilon l}(r)Y_{lm}(\theta,\phi) ; \tag{34b}$$

again we have omitted the labels m and ϵ. The total atomic wave function (32),

$$\Psi_{\epsilon lm}(\vec{r}) = \cos\delta_l f_l(\vec{r}) - \sin\delta_l g_l(\vec{r}) \tag{35}$$

$$= [e^{im\phi}(2\pi)^{-1/2}]P_{lm}(\cos\theta)[\cos\delta_l f_{\epsilon l}(r) - \sin\delta_l g_{\epsilon l}(r)] , \tag{36}$$

is energy normalized over the range (2) by Eqs. (33a) and (33b), as was $\psi_{\epsilon lm}(\vec{r}) \equiv f_l(r)$ itself in Sec. II A. $\Psi_{\epsilon lm}$ may therefore be treated on the same footing as $\psi_{\epsilon lm}$ upon passing to the Coulomb-Stark region via the coordinate transformation(s) between energy-normalized spherical and parabolic functions.

A. Core effects and Green's function

The net effect of the core on the spherical solutions $\Psi_{\epsilon lm}$ is contained in the phase shifts δ_l. The coefficient $\tan\delta_l$ in Eq. (32) may be viewed as a matrix element of a diagonal reaction operator K, defined on the core boundary $r = r_0$ and operating on the regular solution

$$|\epsilon lm\rangle \equiv \psi_{\epsilon lm}/N_{\epsilon l} ,$$

Eqs. (12) and (34a):

$$N_{\epsilon l'}\langle \epsilon l'm \,|\, K \,|\, \epsilon lm \rangle N_{\epsilon l} = -\delta_{l'l}\pi^{-1}\tan\delta_l . \tag{37}$$

The diagonality symbol $\delta_{l'l}$ in this equation applies only to alkali-metal atoms with a closed-shell core; it should be replaced for other atoms whose reaction operator is not diagonal in a basis of spherical waves. The normalization coefficient

$$\cos\delta_l = (1 + \tan^2\delta_l)^{-1/2}$$

is set positive by taking the quantum defects μ_l on the branch

$$-\tfrac{1}{2} < \mu_l < +\tfrac{1}{2} , \tag{38}$$

i.e.,

$$\mu_l \rightarrow (\mu_l + \tfrac{1}{2})(\text{mod}\,1) - \tfrac{1}{2} .$$

This choice also ensures that the regular spherical and parabolic functions are defined with the correct sign at $r \rightarrow 0$, Eqs. (6) and (12), and therefore transform according to Eqs. (16a) and (16b).

The irregular solution (34b) arises because the core potential departs from a pure Coulomb potential at $r < r_0$. The departure from $-1/r$ acts as an inhomogeneity whose effect is propagated by the standing-wave Coulomb Green's function

$$G^c(\vec{r},\vec{r}') = \pi \sum_{l,m} g_l(\vec{r})f_l(\vec{r}') ,$$

$$r' < r \ll F^{-1/2} \tag{39}$$

a solution of the Schrödinger equation for the Coulomb potential alone. The Green's function (39) is specified uniquely by our choice of boundary conditions, namely, regularity at the origin for f_l and a 90° phase lag of g_l with respect to f_l in region (2). Furthermore, the Coulomb degeneracy in region (2) implies that the spherical and parabolic forms of $G^c(\vec{r},\vec{r}')$ must *coincide* there, as pointed out by Fano.[13]

We thus require the spherical Green's function (39) to be equal to its analog in parabolic coordinates,

$$G^c(\vec{r},\vec{r}') = 2 \sum_{\beta,m} \chi_\beta^F(\vec{r})\psi_\beta^F(\vec{r}')/W_\eta(\Upsilon_\beta^F, \overline{\Upsilon}_\beta^F) ,$$

$$\eta' < \eta \ll F^{-1/2} . \tag{40}$$

In analogy to Eq. (39) the right-hand side of Eq. (40) is constructed with the regular parabolic eigenfunction $\psi_\beta^F \propto \Upsilon_\beta^F(\eta)$ from Sec. II A, Eq. (4), and with a second parabolic function irregular at $\eta = 0$, $\chi_\beta^F \propto \overline{\Upsilon}_\beta^F(\eta)$, with the same eigenvalue β as ψ_β^F:

$$\chi_{\epsilon n_1 m}^F = \chi_\beta^F(\xi,\eta,\phi) = \frac{e^{im\phi}}{\sqrt{2\pi}}\Xi_\beta^F(\xi)\overline{\Upsilon}_\beta^F(\eta) . \tag{41}$$

The function $\overline{\Upsilon}_\beta^F(\eta)$ lags $90°$ in phase behind $\Upsilon_\beta^F(\eta)$ for $1 \ll \eta \le F^{-1/2}$, that is, only *within region* (2). This relationship parallels the large-r boundary condition on $g_{el}(r)$ expressed by Eqs. (33). On the other hand, Υ and $\overline{\Upsilon}$ are continuum normalized at $\eta \to \infty$; asymptotically, they oscillate like Airy functions with a different phase relationship, discussed below.

We shall now verify that the Green's functions (39) and (40) indeed satisfy the same boundary condition in region (2). To this end we consider a nar-

row cylinder about the negative z axis, such that

$$\theta \approx \pi ,$$

$$P_{lm}(\theta) \propto \sin^m\theta \approx (\pi - \theta)^m ,$$

$$\xi = r(1 + \cos\theta) \approx \tfrac{1}{2}r(\pi - \theta)^2 ,$$

and

$$\eta = r(1 - \cos\theta) \approx 2r \ll F^{-1/2} .$$

The regular hydrogenic functions in this region reduce to confluent hypergeometric functions,[15]

$$f_l(\vec{r}) = N_{\epsilon lm}[e^{im\phi}e^{-r/v}(\pi - \theta)^m]r^l F(-v + l + 1, 2l + 2; 2r/v) \tag{42}$$

and

$$\psi_\beta(\vec{r}) = N_{\epsilon\beta m}[e^{im\phi}e^{-r/v}(\pi - \theta)^m]r^m F(-\beta_2 v + \tfrac{1}{2}m + \tfrac{1}{2}, m + 1; \eta/v) , \tag{43}$$

where we have used

$$(\xi\eta)^{1/2m} \approx [r^2(\pi - \theta)^2]^{1/2m} ,$$

$$v = (-2\epsilon)^{-1/2}, \quad F(\ldots; \xi/v) \approx 1 ,$$

and where numerical factors are lumped into $N_{\epsilon lm}$ and $N_{\epsilon\beta m}$. The factors in brackets are the same in Eqs. (42) and (43). The remaining factors are analytic functions in the variables $2r/v$ and η/v, respectively, which *coincide within our narrow cone*. We have seen in Eq. (16a) how the function (43) could be matched by a superposition of the functions (42). By the same token an irregular solution lagging in phase by $90°$ with respect to (43) will be matched to a superposition of solutions lagging in phase by $90°$ with respect to (42). The uniqueness and separability of the Green's function in the pure-Coulomb region guarantee that the matching achieved in the narrow cone applies off the axis as well. The spherical and parabolic Green's functions thus coincide throughout region (2) *independently* of the Stark field.

This comparison of Green's functions differs from Fano's treatment of nonhydrogenic Stark spectra[13] in the following respect. The Green's function is defined in Ref. 13 through its eigenfunction expansion—i.e., as a principal part integral over all ϵ—which is brought to the form of Eq. (39) [or (40)] only at $r \to \infty$ [$\eta \to \infty$], where the Stark field dominates. However, we have seen that the irregular functions must be defined with respect to the regular ones in the pure-Coulomb zone (2). Thus, the approach of Ref. 13 is incomplete, insofar as it ignores the essential barrier effects below threshold that produce interferences between parabolic eigen-

functions at $\eta \to \infty$, as will be seen in Sec. III C. Fano's main contribution lies in the identification of the Coulomb Green's function in bases of different symmetries.

Normalization per unit energy of the parabolic functions ψ_β^F and χ_β^F does depend on the field strength F through barrier effects outside region (2). If we begin with $\Upsilon_\beta^F(\eta)$ and $\overline{\Upsilon}_\beta^F(\eta)$ for $\eta \ll F^{-1/2}$ in their WKB forms, Eqs. (33a) and (33b) [with $k(r)$ replaced by

$$k(\eta) = (-\tfrac{1}{4}m^2/\eta^2 + \beta_2/\eta + \tfrac{1}{2}\epsilon + \tfrac{1}{4}F\eta)^{1/2}] ,$$

propagation across the barrier modifies their phases and amplitudes[10]:

$$\Upsilon_\beta^F(\eta) \xrightarrow[\eta \to \infty]{} R_\beta^F[2/\pi k(\eta)]^{1/2}\sin\left[\int^\eta k(\eta')d\eta' + \tfrac{1}{4}\pi + \delta_\beta^F\right],$$

$$\tag{44a}$$

$$\overline{\Upsilon}_\beta^F(\eta) \xrightarrow[\eta \to \infty]{} S_\beta^F[2/\pi k(\eta)]^{1/2}\sin\left[\int^\eta k(\eta')d\eta' + \tfrac{1}{4}\pi + \delta_\beta^F - \gamma_\beta^F\right].$$

$$\tag{44b}$$

The asymptotic relative phase shift γ_β^F differs in general from $\tfrac{1}{2}\pi$ but lies in the range $0 < \gamma_\beta^F < \pi$. (The absolute phase shift δ_β^F is discussed in Ref. 10 but is irrelevant here.) The ratio of amplitudes of $\Upsilon_\beta^F(\eta)$ [or $\overline{\Upsilon}_\beta^F(\eta)$] at small and large η is $(R_\beta^F)^{-1}$ [or $(S_\beta^F)^{-1}$]. In order to regain the continuum normalizaton $[2/\pi k(\eta)]^{1/2}\sin(\cdots)$ appropriate to the ionization region $\eta \to \infty$, we multiply Eqs. (44) by these ratios to obtain

$$\langle \psi^F_{\epsilon'\beta'm'} \mid \psi^F_{\epsilon\beta m} \rangle = \langle \chi^F_{\epsilon'\beta'm'} \mid \chi^F_{\epsilon\beta m} \rangle = \delta(\epsilon' - \epsilon)\delta_{\beta'\beta}\delta_{m'm} \ , \tag{45}$$

$$\langle \psi^F_{\epsilon'\beta'm'} \mid \chi^F_{\epsilon\beta m} \rangle = \langle \chi^F_{\epsilon'\beta'm'} \mid \psi^F_{\epsilon\beta m} \rangle = \cos\gamma^F_\beta \delta(\epsilon' - \epsilon)\delta_{\beta'\beta}\delta_{m'm} \ , \tag{46}$$

$$W_\eta(\Upsilon^F_\beta, \overline{\Upsilon}^F_\beta) = (2/\pi)\sin\gamma^F_\beta = (2/\pi)(R^F_\beta S^F_\beta)^{-1} \ . \tag{47}$$

Explicit expressions for R^F_β, S^F_β, and γ^F_β are given in Appendix A; we note here the following properties of the amplitudes and phases, illustrated schematically in Fig. 6: (a) at energies sufficiently above the barrier top $(\epsilon \gtrsim 0)$, R^{-1} and S^{-1} approach unity and γ^F_β reduces to $\frac{1}{2}\pi$ for all β; (b) below the barrier top, $\epsilon < \epsilon_c$, R^{-1} and S^{-1} are exponentially small and $\gamma^F_\beta \gtrsim 0$ or $\lesssim \pi$, except that (c) near a resonance R^{-1} is very large with (approximately) Lorentzian profile and $\widetilde{\gamma}^F_\beta$ rapidly increases by $\approx \pi$ through its value $\gamma^F_\beta = \frac{1}{2}\pi$ at the resonance.

The equivalence of the Green's functions (39) and (40) now serves to relate the irregular functions in region (2) with the boundary conditions and normalization conventions prescribed above:

$$G^c(\vec{r}, \vec{r}') = \pi \sum_{l,m} g_l(\vec{r}) f_l(\vec{r}') = \pi \sum_{\beta m} \chi^F_\beta(\vec{r})\csc\gamma^F_\beta\psi^F_\beta(\vec{r}')$$

$$= \pi \sum_{\beta, m} [S^F_\beta\chi^F_\beta(\vec{r})][R^F_\beta\psi^F_\beta(\vec{r}')], \quad r' < r \ll F^{-1/2} \ . \tag{48}$$

The role of the Wronskian (47) in the Green's function (40), performed in (48) by $\csc\gamma^F_\beta$ or $S^F_\beta R^F_\beta$, is to reduce the parabolic functions $\overline{\Upsilon}^F_\beta(\eta)$ and $\Upsilon^F_\beta(\eta)$ to the same normalization as $g_l(\vec{r})$ and $f_l(\vec{r})$, thus removing any barrier effect from the Coulomb Green's function. [The Stark field exerts only an implicit effect by determining the spectrum of eigenvalues $\beta(\epsilon, F; n_1, m)$.] The transformation between the sets $\{g_l\}$ and $\{\chi^F_\beta\}$ follows immediately upon substituting the transformation between $\{f_l\}$ and $\{\psi^F_\beta\}$ into Eq. (48). In the present notation
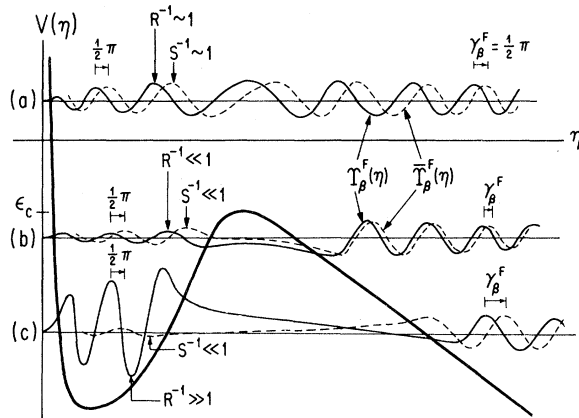

FIG. 6. Wave functions $\Upsilon^F(\eta)$ and $\overline{\Upsilon}^F(\eta)$ (schematic) in the potential $V(\eta) = \frac{1}{4}(m^2 - 1)/\eta^2 - \beta_2/\eta - \frac{1}{4}F\eta$ $(\beta_2 > 0)$, showing different barrier effects. Amplitudes fixed by energy normalization at $\eta \to \infty$; relative phase $\frac{1}{2}\pi$ fixed at $\eta \ll F^{-1/2}$. Amplitudes $(R^F_\beta)^{-1}$ and $(S^F_\beta)^{-1}$ induced at $\eta \ll F^{-1/2}$; relative phase γ^F_β induced at $\eta \to \infty$. (a) $\epsilon \gg \epsilon_c$, weak barrier reflection. (b) $\epsilon < \epsilon_c$, barrier tunneling off resonance. (c) $\epsilon < \epsilon_c$, Υ^F_β quasibound at resonance in the potential well.

Eqs. (16a) and (16b) read

$$\psi^F_\beta(\vec{r}) = \sum_l U_{\beta l}f_l(\vec{r}) \ , \tag{49a}$$

$$f_l(\vec{r}) = \sum_\beta (U^{-1})_{l\beta}\psi^F_\beta(\vec{r}) \ ; \tag{49b}$$

Eq. (48) then yields

$$\chi^F_\beta(\vec{r}) = \sum_l \sin\gamma^F_\beta(\widetilde{U}^{-1})_{\beta l}g_l(\vec{r}) \ , \tag{50a}$$

$$g_l(\vec{r}) = \sum_\beta \widetilde{U}_{l\beta}\csc\gamma^F_\beta\chi^F_\beta(\vec{r}) \tag{50b}$$

with constant values of ϵ and m implicit throughout. Note how the transformation UR in Eqs. (48) and (49) is replaced by $(\widetilde{U}R)^{-1}$ in Eqs. (50), which equals UR only for $F = 0$.

B. Photoionization and generalized density-of-states matrix

Our treatment of photoionization for alkali-metal atoms now follows as a generalization of Secs. II C and II D for H. We consider photoabsorption by an atom in an initial state Ψ_i that is confined to $r \leq r_0$. Ψ_i may be the ground state or a low-lying excited state. Following photoabsorption, the final-state spherical wave function $\Psi_{\epsilon l m}(\vec{r})$, Eq. (35), evolves through the Coulomb zone (2) and into the ionizing region, $\eta \to \infty$, where it must be continuum normalized in the parabolic basis. We accordingly replace the basis functions $\{f_l(\vec{r}), g_l(\vec{r})\}$ in Eq. (35) by their respective expansions (49b) and (50b) into the energy-normalized basis functions $\{\psi^F_\beta(\vec{r}), \chi^F_\beta(\vec{r})\}$, giving, for $r > r_0$,

$$\Psi_{\epsilon lm}(\vec{r}) = \cos\delta_l \sum_\beta (U^{-1})_{l\beta} \psi_\beta^F(\vec{r}) - \sin\delta_l \sum_\beta \tilde{U}_{l\beta} \csc\gamma_\beta^F \chi_\beta^F(\vec{r}) \tag{51}$$

$$= [e^{im\phi}(2\pi)^{-1/2}] \sum_\beta \Xi_\beta^F(\xi)\{[\cos\delta_l(U^{-1})_{l\beta}]\Upsilon_\beta^F(\eta) - [\sin\delta_l \tilde{U}_{l\beta}\csc\gamma_\beta^F]\bar{\Upsilon}_\beta^F(\eta)\} . \tag{52}$$

In matrix notation, Eq. (51) reads

$$\Psi = \cos\delta \, U^{-1}\psi^F - \sin\delta \, \tilde{U}\csc\gamma \, \chi^F , \tag{53}$$

where the sets of functions $\{\Psi_l\}$, $\{\psi_\beta^F\}$, and $\{\chi_\beta^F\}$ form column vectors and trigonometric functions represent diagonal matrices. Each parabolic channel in the superposition (52) contains one eigenfunction $\Xi_\beta^F(\xi)$ and a linear combination of $\Upsilon_\beta^F(\eta)$ and $\bar{\Upsilon}_\beta^F(\eta)$, as Eq. (36) contained one function of $\cos\theta$ and a combination of $f_{\epsilon l}(r)$ and $g_{\epsilon l}(r)$.

In order to orthonormalize the set $\{\Psi_l\}$, Eq. (53), we construct the overlap matrix $\langle \Psi_{\epsilon'l'm'} | \Psi_{\epsilon lm} \rangle$:

$$\langle \Psi' | \Psi \rangle = \cos\delta \, U^{-1}\tilde{U}^{-1}\cos\delta + \sin\delta \, \tilde{U}\csc^2\gamma \, U\sin\delta - \cos\delta \, U^{-1}\cos\gamma \, \csc\gamma \, U\sin\delta$$

$$- \sin\delta \, \tilde{U}\csc\gamma \, \cos\gamma \, \tilde{U}^{-1}\cos\delta$$

$$= (\cos\delta - \sin\delta \, \tilde{U}\cot\gamma \, U)(\tilde{U}U)^{-1}(\cos\delta - \tilde{U}\cot\gamma \, U\sin\delta) + \sin\delta \, \tilde{U}U\sin\delta , \tag{54}$$

where we have taken the transpose of the coefficients in $| \Psi \rangle$; an overall factor $\delta_{m'm}\delta(\epsilon'-\epsilon)$ is understood. In the first line of Eq. (54) we have used (1) the orthogonality of the eigenfunctions $\Xi_\beta^F(\xi)$, and (2) the overlap integrals for ψ_β^F and χ_β^F, Eqs. (45) and (46); in the second line, (3) the identity $\csc^2\gamma = 1 + \cot^2\gamma$. Note that each channel in Eq. (54) includes a pair of *interference* terms between ψ_β^F and χ_β^F, proportional to $\cos\gamma_\beta^F$. These terms vanish in the special case of hydrogen, where all $\delta_l = 0$, and we recover Eq. (25).

Core effects appear in Eq. (54) only through the short-range phase shifts δ_l. The Stark effect is manifest instead through hydrogenic parameters determined by the potential [Eq. (1)]: (1) the amplitudes of barrier penetration, $(R_\beta^F)^{-1}$, appearing in the normalization coefficient N_β^F in $U_{\beta l}$ [Eqs. (21) and (44a)], and (2) the asymptotic phase shifts γ_β^F. The hydrogenic DOS transformation, $H^F = \tilde{U}U$, contains only information on the intensity in each parabolic channel; its terms are $\propto (R_\beta^F)^{-2}$. Phase information is contained instead in a second hydrogenic constituent of Eq. (54), which we designate as a companion to H^F:

$$h_{l'l}^F \equiv \delta_{m'm} \sum_\beta U_{\beta l'}^{\epsilon m'} U_{\beta l}^{\epsilon m}\cot\gamma_\beta^F \tag{55a}$$

or

$$h^F = \tilde{U}\cot\gamma \, U , \tag{55b}$$

analogous to Eq. (23a) or (23b). Near a resonance, H^F and h^F will be seen to vary with energy as a pair of absorption and dispersion curves.

The cross section for photoionization of an alkali-metal atom is now given as a generalization of the hydrogenic expression (31):

$$\sigma^F(\epsilon) = \sum_{l',l} [\langle \Psi' | \Psi \rangle^{-1}]_{l'l}\sigma_{l'l}(\epsilon)$$

$$= \mathrm{Tr}[D^F\sigma(\epsilon)] , \tag{56}$$

with zero-field dipole matrix elements contained in

$$\sigma_{l'l}(\epsilon) = (4\pi^2\alpha)\hbar\omega \langle \Psi_i | r_m | \Psi_{\epsilon l'm} \rangle \langle \Psi_{\epsilon lm} | r_m | \Psi_i \rangle \tag{57}$$

and with the Stark effect embodied in the DOS matrix

$$D^F \equiv \langle \Psi' | \Psi \rangle^{-1} = \{(\cos\delta - \sin\delta \, h^F)(H^F)^{-1}(\cos\delta - h^F\sin\delta) + \sin\delta \, H^F\sin\delta\}^{-1} . \tag{58}$$

Equations (56)–(58) are the central results of this paper. Our study of various spectra near threshold will henceforth focus on the modulating factors $D_{l'l}^F$, since the factors in Eq. (57) vary very slowly within, e.g., 0.1 eV of threshold. The matrix inversions in Eq. (58) are restricted to the $l' \times l$ subspace where $\delta_l \neq 0$—which is $0 \leq l \leq 2$ or 3 for alkalis—so

manipulation of Eq. (58) requires only a modest amount of matrix algebra (Appendix B). Numerical computation of $\sigma^F(\epsilon)$ is limited to a few matrix elements $H_{l'l}^F(\epsilon)$ and $h_{l'l}^F(\epsilon)$, which in turn depend only on $a_{\beta l}^{\epsilon m}$ and on a few hydrogenic parameters, $\beta_{\epsilon n_1 m}^F$, N_β^F, and γ_β^F (see Appendix A). The number of parabolic channels that contribute significantly to H^F

and h^F is in practice[10] $\lesssim [F(\text{a.u.})]^{-1/4}$ $=47[F(\text{kV/cm})]^{-1/4}$, e.g., ≈ 26 channels for $F=10$ kV/cm.

C. $D_{l'l}^F$ and Spectral Profiles

We present here a brief study of the matrix elements $D_{l'l}^F$ of Eq. (58), which modulate the slowly varying zero-field cross sections $\sigma_{l'l}(\epsilon)$. When all $\delta_l=0$, Eq. (58) reduces to Eq. (27) for the hydrogenic spectrum $H_{l'l}^F$, indicated by the solid lines in Figs. 1(a), 2(a), 3, and 4 for $F=77$ kV/cm and for various values of m and (l',l). We regard the quantities $D_{l'l}^F$ as variants of the hydrogenic spectrum $H_{l'l}^F$. The deviation of the matrix D^F from H^F is a function of the set of quantum defects $\mu_l=\delta_l/\pi$ [with the restriction (38)] and involves the hydrogenic quantities $h_{l'l}^F$ as well.

By way of example, we illustrate the modulating factors for Na by the dashed lines in Figs. 1−4— the observed Na spectra of Refs. 3−5 will be discussed in Sec. IV. The values

$$\mu_0=1.350\rightarrow+0.350 \ ,$$

$$\mu_1=0.856\rightarrow-0.144 \ ,$$

$$\mu_2=0.014, \ \mu_l\geq3\approx0 \tag{59}$$

were taken from experimental data[23] for the highly excited levels of Na I and were assumed to be energy independent. Note that (A) the oscillations at $\epsilon\geq0$ are *diminished* in magnitude in every case and *inverted* in Fig. 3(a), and (B) the peaks at $\epsilon<0$ are broadened and asymmetric with interference minima on one side or the other in a given spectrum, but with the line shapes varying among the different spectra. We shall discuss first $H^F(\epsilon)$ and $h^F(\epsilon)$ and then describe how these building blocks are combined by different values of $\{u_l\}$ to generate the observed profiles.

$H_{11}^F(\epsilon)$ and $h_{11}^F(\epsilon)$ are shown together in Fig. 1(b) for $m=0$ and in Fig. 2(b) for $m=1$. Near or above $\epsilon=0$, H_{11}^F oscillates about unity with $|H_{11}^F-1|\ll1$ (see Sec. II C). In general $H_{l'l}^F$ oscillates about unity (zero) for $l'=l(l'\neq l)$ with $|H_{l'l}^F-\delta_{l'l}|\sim O(0.1)$, as shown in Figs. 3(a)−3(c) for $(l',l)=(0,0),(2,0),(2,2)$. The function $h_{l'l}^F$, on the other hand, quickly vanishes at $\epsilon\geq0$. In this range all the relative phase shifts in Eq. (55a) approach $\gamma_\beta^F=\frac{1}{2}\pi$ [see Fig. 6(a)], since ϵ is far enough above the barrier top $\epsilon_c=-2[(1-\beta)F]^{1/2}$ in each channel for diffraction by the barrier to have a negligible effect on the wave functions' phases and amplitudes.

(This corresponds to the usual circumstance of a WKB wave function in a single classically accessible region, whose phase accumulation is smooth in a slowly varying potential.) Note the small resonance in Fig. 1(b) at $\epsilon=0$: only in the $n_1=12$ channel, where $\beta_2\geq0$ and the barrier is shallow, is $\epsilon_c\approx0$ and is there any appreciable reflection of $\psi_{\epsilon,n_1=12,m=0}^F$.

Below $\epsilon=0$ there occur instead narrow resonance peaks in $H_{l'l}^F$ at quasibound Stark levels, labeled in Figs. 1−4 by their hydrogenic quantum numbers (n,n_1,n_2,m). For an isolated resonance in the $\bar{\beta}$ $(\bar{n}_1)$ channel we write Eq. (23a) in the form

$$H_{l'l}^F=B_{l'l}^F+(\widetilde{U}_{l'\bar{\beta}}^0 U_{\bar{\beta}l}^0)(R_{\bar{\beta}}^F)^{-2} \ , \tag{60}$$

where we have specified the smoothly varying background

$$B_{l'l}^F=\sum_{\beta\neq\bar{\beta}}\widetilde{U}_{l'\beta}U_{\beta l} \ , \tag{61}$$

which rises from zero at $\epsilon<\epsilon_{\text{ion}}$ to unity at $\epsilon>0$. The "renormalized" transformation coefficient

$$U_{\bar{\beta}l}^0=U_{\bar{\beta}l}R_{\bar{\beta}}^F \tag{62}$$

replaces $U_{\bar{\beta}l}$ in the transformations (49) and (50) if we consider the functions $\Upsilon_{\bar{\beta}}^F(\eta)$ and $\overline{\Upsilon}_{\bar{\beta}}^F(\eta)$ to be energy normalized as in Eqs. (33) and (44), i.e., as in a pure Coulomb potential at $\eta\ll F^{-1/2}$. The factor $R_{\bar{\beta}}^F$ serves to cancel in $U_{\bar{\beta}l}$ the barrier-penetration amplitude R^{-1}—representing the resonance—so $U_{\bar{\beta}l}^0$ varies smoothly through a resonance. The amplitude $R_{\bar{\beta}}^F$ is given in Eq. (A6) in terms of parameters of Appendix A. Near a resonance R^{-2} has a *Lorentzian* profile:

$$(R_{\bar{\beta}}^F)^{-2}=(T^2\cos^2\Delta+T^{-2}\sin^2\Delta)^{-1}$$

$$\xrightarrow[\Delta\rightarrow\pi/2]{} \left.\frac{\frac{1}{2}\Gamma/\pi}{(\epsilon-\epsilon_0)^2+(\frac{1}{2}\Gamma)^2}\frac{d\epsilon}{d(\Delta/\pi)}\right|_{\epsilon_0} \ , \tag{63}$$

where Δ is the WKB phase accumulation modulo π in the potential well of Fig. 6 [Eq. (A3)]; $\epsilon=\epsilon_0$ is the resonance center, corresponding to $\Delta=\frac{1}{2}\pi$; $T\approx2e^\tau\gg1$ is a tunneling amplitude; $d\epsilon/d(\Delta/\pi)$ is approximately the energy spacing between resonances; and the resonance halfwidth

$$\frac{1}{2}\Gamma=T^{-2}d\epsilon/d\Delta\mid_{\epsilon_0} \tag{64}$$

is by assumption $\ll d\epsilon/d(\Delta/\pi)$. We assume for simplicity that all parameters except Δ are nearly

constant within an energy range of several $\frac{1}{2}\Gamma$ about ϵ_0. [This condition will not hold near or above the barrier top; cf. the (12,11,0,0) peak in Fig. 1. Note also that *above* the barrier T actually approaches unity—see Eq. (A7)—so $R^{-2}\rightarrow 1$.]

The behavior of $h_{l'l}^F$ near a resonance varies in tandem with that of $H_{l'l}^F$, Eqs. (60) and (63). From Eq. (55a) we have

$$h_{l'l}^F = b_{l'l}^F + (\tilde{U}_{l'\bar{\beta}}^0 U_{\bar{\beta}l}^0)(R_{\bar{\beta}}^F)^{-2}\cot\gamma_{\bar{\beta}}^F , \qquad (65)$$

with the background

$$b_{l'l}^F = \sum_{\beta\neq\bar{\beta}} \tilde{U}_{l'\beta}\cot\gamma_\beta^F U_{\beta l} \qquad (66)$$

and

$$\cot\gamma_{\bar{\beta}}^F = (T^2 - T^{-2})\sin\Delta\cos\Delta , \quad 0 < \gamma_{\bar{\beta}}^F < \pi \qquad (67)$$

from Eq. (A9). (At $\epsilon > 0$, $T\rightarrow 1$ so $\gamma_{\bar{\beta}}^F\rightarrow\frac{1}{2}\pi$, as stated above.) Thus, with $T\gg 1$, $R^{-2}\cot\gamma$ is the companion *dispersion* curve to the Lorentzian (63):

$$(R_{\bar{\beta}}^F)^{-2}\cot\gamma_{\bar{\beta}}^F = \frac{\sin\Delta\cos\Delta}{\cos^2\Delta + (T^4 - 1)^{-1}}$$

$$\xrightarrow[\Delta\rightarrow\pi/2]{} \frac{(\epsilon_0 - \epsilon)/\pi}{(\epsilon - \epsilon_0)^2 + (\frac{1}{2}\Gamma)^2} \frac{d\epsilon}{d(\Delta/\pi)}\Bigg|_{\epsilon_0} . \qquad (68)$$

The absorption and dispersion curves R^{-2} and $R^{-2}\cot\gamma$ are illustrated in Figs. 1(b) and 2(b), e.g., in the small (11,8,1,1) peak. Note that the maximum of Eq. (68) lies at lower energy than the minimum. This reflects the fact that $\Upsilon_{\bar{\beta}}^F(\eta)$ lags in phase behind $\Upsilon_\beta^F(\eta)$ at $\eta\rightarrow\infty$ by $\gamma_{\bar{\beta}}^F\gtrsim 0$ at $\epsilon < \epsilon_0$ (or $\gamma_{\bar{\beta}}^F\lesssim\pi$ at $\epsilon > \epsilon_0$) [cf. Eq. (67)]. Away from any resonance, $R^{-2}\rightarrow 0$ so $H_{l'l}^F$ just reduces to its background $B_{l'l}^F$; on the other hand, $R^{-2}\cot\gamma\rightarrow\tan\Delta$ and so $|h_{l'l}^F - b_{l'l}^F|$ may be appreciable between resonances. Owing to this circumstance, the mixing of h^F into the nonhydrogenic spectrum (58) will broaden the narrow peaks of H^F.

Case (A) $\epsilon\lesssim 0$, $\epsilon > 0$. Near or above threshold the matrix D^F assumes an especially simple form. As noted above, in this region $|H_{l'l}^F - \delta_{l'l}| \sim O(0.1)$ and $h_{l'l}^F\lesssim |H_{l'l}^F - \delta_{l'l}|$, so to second order in these quantities Eq. (58) reduces to

$$D_{l'l}^F = \delta_{l'l} + (H_{l'l}^F - \delta_{l'l})\cos[\pi(\mu_{l'} + \mu_l)]$$

$$+ h_{l'l}^F\sin[\pi(\mu_{l'} + \mu_l)] . \qquad (69)$$

The cosine factor in the second term in Eq. (69) merely *attenuates* the threshold modulations while

the third term is *asymmetric* at $\epsilon\lesssim 0$ [Eqs. (65) and (68)] and vanishes at $\epsilon > 0$. We see then that the core effect preserves the positions and spacing [8–11] of the hydrogenic series of oscillations $H^F - 1$ but diminishes their depth and possibly *inverts* them according to

$$\frac{D_{l'l}^F - \delta_{l'l}}{H_{l'l}^F - \delta_{l'l}} \begin{cases} > 0 \text{ if } 0 < |\mu_{l'} + \mu_l| < \frac{1}{2} , \\ \approx 0 \text{ if } \mu_{l'} + \mu_l\approx\pm\frac{1}{2} , \\ < 0 \text{ if } \frac{1}{2} < |\mu_{l'} + \mu_l| < 1 . \end{cases} \qquad (70)$$

The condition (70) is illustrated by the dashed lines in Figs. 1 and 3 ($m = 0$). Referring to the quantum defects (59) for Na, the modulations in Fig. 1(a) ($2\mu_1 = -0.29$) and Fig. 3(b) ($\mu_2 + \mu_0 = 0.36$) are simply shallower than for H, but are inverted in Fig. 3(a) ($2\mu_0 = 0.70$). (D_{22}^F in Fig. 3(c) is hardly affected since $2\mu_2 = 0.03\approx 0$.) Such an inversion would give rise to an *apparent* shift of the hydrogenic oscillations by $180°$ in an experimental spectrum if their slight asymmetry were overlooked. In an $nl_i\rightarrow\epsilon l$ alkali transition with $l' = l$ the zero-field cross section (57) at $\epsilon > 0$ is modulated by

$$D_{ll}^F = 1 + (H_{ll}^F - 1)\cos 2\pi\mu_l . \qquad (71)$$

For example, $5s\rightarrow\epsilon p$ ionizing transitions in Rb[1] ($\mu_1 = 2.65$) should reveal this effect; the expanded spectrum in Fig. 6 of Ref. 1(b) suggests this behavior.

The grosser asymmetry of the dispersive term $h_{l'l}^F$ is evident in all the resonances of D^F below threshold in Figs. 1–4. According to Eq. (68) and the approximation (69), the positions of the smaller peaks' maxima and minima are related by

$$\epsilon_{min}\gtrless\epsilon_{max} \text{ if } \begin{cases} 0 < \mu_{l'} + \mu_l < 1 \\ 0 > \mu_{l'} + \mu_l > -1 \end{cases} \qquad (72)$$

and there is no asymmetry if $\mu_{l'} + \mu_l = 0$. For example, the interference dips in Figs. 3(a)−3(c) and 4(a)−4(b) are all on the high-energy side of their peaks, whereas the minima in Figs. 1(a) and 2(a) ($2\mu_1 < 0$) are on the opposite side. The asymmetry condition (72) still holds, in general, when the peaks are very sharp (see below). Thus, a knowledge of the quantum defects suffices to predict both (a) the sign of the peaks' asymmetry in the cross section (56) as well as (b) the depth of the threshold modulations in a nonhydrogenic atom.

Case (B) $\epsilon < 0$. The sharp resonances below threshold cannot be described by Eq. (69) since $H^F - 1$ and $|h^F| \gg 0$. The most general treatment

of the matrix equation (58) for $D_{l'l}^F$ involves the solution of an eigenvalue problem, detailed in Appendix B, whose dimension is no larger than the number of nonzero quantum defects $\mu_l = \delta_l/\pi$. Thus, all the dashed curves for Na in Figs. 1—4 involve only matrix elements $H_{l'l}^F$ and $h_{l'l}^F$ with $l',l \leq 2$ [cf. Eq. (59)]. Although the matrix manipulations in the solution of Eq. (58) are computationally simple, the exact algebraic expressions for $D_{l'l}^F$ with even just two $\mu_l \neq 0$ are cumbersome. We shall therefore discuss the profile of an isolated resonance as a function of a single nonvanishing $\mu_l \equiv \mu_1$; though unrealistic, this example adequately reflects the qualitative features of the alkali-metal spectra shown in the figures.

The simplest expression is for the matrix element with $l' = l = 1$:

$$D_{ll}^F = H_{ll}^F \frac{1 + \tan^2 \delta_l}{(1 - h_{ll}^F \tan\delta_l)^2 + (H_{ll}^F \tan\delta_l)^2} \qquad (73)$$

or equivalently

$$D_{ll}^F = \csc^2\delta_l \, \mathrm{Im}\{[\cot\delta_l - (h_{ll}^F + iH_{ll}^F)]^{-1}\} \ . \qquad (74)$$

Equation (73) is plotted versus $(\epsilon - \epsilon_0)/\frac{1}{2}\Gamma$ in Fig. 7(b) for various values of μ_1. Figure 7(a) (first panel) shows the pair of absorption and dispersion
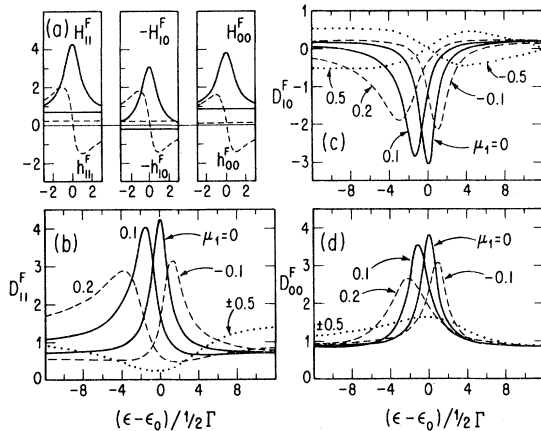

FIG. 7. $D_{l'l}^F$ vs $(\epsilon - \epsilon_0)/\frac{1}{2}\Gamma$ for a single $\delta_l/\pi = \mu_l \equiv \mu_1 \neq 0$. (a) Hydrogen matrix elements $l',l = 1$ or 0 used in Eq. (58). —— Lorentzian $H_{l'l}^F$ [Eq. (60)] with $B_{11} = 0.70$, $B_{10} = 0.20$, $B_{00} = 0.86$; ---- dispersion $h_{l'l}^F$ [Eq. (65)] with $b_{11} = 0.25$, $b_{10} = -0.20$, $b_{00} = 0.10$; ($T^2 = 31.5$, $U_{\beta1}^0 = -0.34$, $U_{\beta0}^0 = 0.31$). (b) D_{11}^F for different μ_1, Eq. (73). Values of q and G calculated from Eqs. (80)—(86) for various μ_1:

μ_1	0	0.1	−0.1	0.2	±0.5
q	∞	−4.0	+4.8	−1.6	+0.4
G	1	1.3	1.2	2.4	5.5.

(c) D_{10}^F and (d) D_{00}^F for same μ_1 as in (b).

curves H_{11}^F and h_{11}^F used to plot D_{11}^F in Fig. 7(b). [The relevant parameters of H^F and h^F in Eqs. (60)—(68) correspond roughly to the (11,9,1,0) resonance of Fig. 1, with $\Gamma = 1.28 \times 10^{-5}$ a.u.] For small values of $H_{11}^F - 1$ and h_{11}^F, Eq. (73) reduces to Eq. (69); if $\delta_l = 0$, we recover $D_{11}^F = H_{11}^F$ for hydrogen. The asymmetry of D_{11}^F comes from the term $(1 - h_{11}^F \tan\delta_1)^2$ in the denominator of Eq. (73), since this term is not even with respect to $\epsilon = \epsilon_0$. Note, however, that the reflection $\mu_1 \to -\mu_1$ does not produce the reflection

$$D_{11}^F(\epsilon - \epsilon_0) \to D_{11}^F(\epsilon_0 - \epsilon)$$

in Figs. 7(b)—7(d), since h_{11}^F contains the background term b_{11}^F [Fig. 7(a)] and so is not exactly odd about ϵ_0.

A nonzero value of μ_1 also affects the resonances $D_{l'l}^F$ with l' and/or $l \neq 1$, but to a lesser extent than it affects D_{11}^F itself. Figures 7(c) and 7(d) show D_{10}^F and D_{00}^F for the same μ_1 used in Fig. 7(b); the functions H_{10}^F, h_{10}^F, H_{00}^F, h_{00}^F are also shown in Fig. 7(a). Note that these curves are broadened but less asymmetric than the curves D_{11}^F.

The interference effects that give rise to the asymmetric profiles of $D_{l'l}^F$ stem from the factor $\cot\gamma_\beta^F$ [Eqs. (65) and (67)] in the resonance channel of $h_{l'l}^F$. If $\sin\delta_l > 0$ in the total wave function $\Psi_{\epsilon lm}(r)$, Eq. (51), ψ_β^F and χ_β^F interfere almost entirely constructively (or destructively) at $\eta \to \infty$, where $\gamma_\beta^F < \frac{1}{2}\pi$ (or $\gamma_\beta^F > \frac{1}{2}\pi$), so $\langle \Psi_{l'} | \Psi_l \rangle$ is small (or large) when $\epsilon < \epsilon_0$ (or $\epsilon > \epsilon_0$); if $\sin\delta_l < 0$ the opposite is true. Thus, the asymmetry condition (72) holds for all resonances with nearly constant parameters T and Γ in each spectrum

$$D_{l'l}^F(\epsilon) = [\langle \Psi' | \Psi \rangle^{-1}]_{l'l} \ .$$

Any nonzero quantum defect μ_l will affect all channels of $D_{l'l}^F$, with either the same or different l' and l, since the overlap matrix $\langle \Psi_{l'} | \Psi_l \rangle$ mixes all l channels.

1. Beutler-Fano profiles

The archetypal expression (73) can be cast into the form of a Fano profile[24] under the resonance conditions stated above for $(R_\beta^F)^{-2}$. We seek the parametrization

$$D_{ll}^F = A + a \frac{(\varepsilon - \varepsilon_0 + Gq)^2}{(\varepsilon - \varepsilon_0)^2 + G^2} \ , \qquad (75)$$

where

$$\varepsilon = (\epsilon - \epsilon_0)/\frac{1}{2}\Gamma \qquad (76)$$

measures the energy with respect to the center of the hydrogen-Stark resonance in units of its halfwidth, $\varepsilon_0 \frac{1}{2}\Gamma$ is the energy shift of the resonance from ϵ_0, G measures the relative broadening of $\frac{1}{2}\Gamma$, q is the usual asymmetry parameter, and A and a are positive constants. These parameters are all expressible in terms of $\delta_l = \pi\mu_l$ and parameters of H_{ll}^F and h_{ll}^F. We abbreviate

$$H_{ll}^F = B + cR^{-2} , \tag{77a}$$

$$h_{ll}^F = b + cR^{-2}\cot\gamma , \tag{77b}$$

in Eqs. (60) and (65), with $c = (U_{\beta l}^0)^2$ and with indices omitted. We will also use an important identity stemming from Eqs. (63) and (67):

$$R'^2 = (\cos\delta' - \sin\delta' R^{-2}\cot\gamma)^2 R^2 + \sin^2\delta' R^{-2}$$

$$\equiv T^2\cos^2(\Delta + \delta') + T^{-2}\sin^2(\Delta + \delta') , \tag{78}$$

which coincides with Eq. (63) for R^2 with the replacement $\Delta \rightarrow \Delta + \delta'$. (Equation (78) also follows from the identity $\csc\gamma \equiv RS$ [Eq. (47)] and the definitions of the amplitudes R [Eq. (63)] and S (R with $\Delta \rightarrow \Delta - \frac{1}{2}\pi$).)

Inserting Eqs. (77a) and (77b) into Eq. (73) for D_{ll}^F, we find after rearranging terms that

$$D_{ll}^F = B[(\cos\delta_l - b\sin\delta_l)^2 + (B^2 + c^2)\sin^2\delta_l]^{-1}\left[\frac{\varepsilon^2 + 1 + cT^2/B}{(\varepsilon - \varepsilon_0)^2 + G^2}\right] , \tag{83}$$

a form readily identified with Eq. (75). The energy shift of the resonance (in units of $\frac{1}{2}\Gamma$) is

$$\varepsilon_0 = -\delta_l' T^2[1 + (B/c)^2\sin^2\delta_l']^{-1} , \tag{84}$$

which is smaller in magnitude than ε'. The phase shift δ_l' thus plays a role analogous to δ_l in a Rydberg atom by shifting the hydrogenic Stark spectrum in energy by

$$\varepsilon_0(\tfrac{1}{2}\Gamma) \propto (\delta_l'/\pi)d\epsilon/d(\Delta/\pi) ,$$

i.e., with a "quantum defect" $\mu_l' = \delta_l'/\pi$ and with level spacing $n'^{-3} = d\epsilon/d(\Delta/\pi)$. The broadened resonance halfwidth G is given in units of $\frac{1}{2}\Gamma$ by

$$G^2 = 1 + 2x + [(\delta_l'/\sin\delta_l')^2 - 1]x^2 ,$$

$$x = |\varepsilon_0/\delta_l'| \frac{B}{c}\sin^2\delta_l' , \tag{85}$$

and q is the solution with the same sign as ε_0 of the equation

$$q^2 - \left[\frac{\varepsilon_0^2 - G^2 + 1 + cT^2/B}{\varepsilon_0 G}\right]q - 1 = 0 . \tag{86}$$

$$D_{ll}^F = \left[\frac{\sin^2\delta'}{c\sin^2\delta_l}\right]\left[\frac{cR'^2 + B\sin^2\delta'}{BR^2 + c} + \frac{B}{c}\sin^2\delta'\right]^{-1} , \tag{79}$$

where δ_l determines another phase shift,

$$\delta_l' = \tan^{-1}\left[\frac{c}{\cot\delta_l - b}\right] , \quad -\tfrac{1}{2}\pi < \delta_l' < \tfrac{1}{2}\pi . \tag{80}$$

The Lorentzians (63) and (78),

$$R^{-2} = \frac{T^2}{\varepsilon^2 + 1} , \tag{81a}$$

$$R'^{-2} = \frac{T^2}{(\varepsilon - \varepsilon')^2 + 1} , \tag{81b}$$

have the same width Γ [Eqs. (64) and (76)] but R'^{-2} is shifted from $\varepsilon = 0$ by

$$\varepsilon' = -\frac{\delta_l' d\epsilon/d\Delta}{\frac{1}{2}\Gamma} = -T^2\delta_l' ; \tag{82}$$

ε' marks the maximum of D_{ll}^F for $T \gg 1$. Equation (79) can now be further recast into a simple ratio of Lorentzians:

When δ_l is small such that $\cot\delta_l \gg T^2, B, b, c$, Eq. (86) simplifies to

$$q \approx -\cot\delta_l/B . \tag{86'}$$

Finally, the weighting factor a and the background A of Eq. (75) are

$$a = \left[\frac{\varepsilon_0}{Gq}\right]B[(\cos\delta_l - b\sin\delta_l)^2$$
$$+ (B^2 + c^2)\sin^2\delta_l]^{-1} \tag{87}$$

and

$$A = \left[\frac{Gq}{\varepsilon_0} - 1\right]a . \tag{88}$$

The set of five parameters $\{\varepsilon_0, G, q, a, A\}$, Eqs. (84)–(88), completely characterizes the Fano profile (75) in terms of the four hydrogen-Stark parameters $\{B, b, c, T^2\}$ plus the alkali-metal quantum defect δ_l/π, along with the related phase shift δ_l', Eq. (80). The values of q and G for the curves of Fig.

7(b) are indicated in the figure caption.

We consider further the case when the background B effectively vanishes, namely, when all parabolic channel functions (except for $\beta = \bar{\beta}$) are ap-

preciably damped at $r \sim r_0$ by barrier tunnelling. With $B = 0$ the parameters of (75) become $\varepsilon_0 = \varepsilon' = -T^2 \delta'$, $G = 1$, $q = \infty$, $A = 0$, and

$$D_{II}^F = aq^2 R'^{-2} = [(\cos\delta_l - b\sin\delta_l)^2 c^{-1} + c\sin^2\delta_l]^{-1} \frac{T^2}{(\varepsilon - \varepsilon')^2 + 1} \ . \tag{89}$$

Therefore, *even with* $\delta_l \neq 0$ an alkali-metal resonance will again be *symmetric:* Eq. (89) is equal to the Lorentzian (81b)—identical to the hydrogen-Stark resonance (81a) but shifted from $\varepsilon = \varepsilon_0$— times a factor representing Eq. (73) [cf. Eq. (58)] with $H^F = c$ and $h^F = b$. We therefore conclude that only those resonances in the "autoionizing" region $0 > \varepsilon > \varepsilon_{\text{ion}} = -\sqrt{4F}$ are asymmetric.

The presence of a background term $B_{l'l}^F$ as well as a nonzero μ_l is thus essential for producing an asymmetric lineshape. This corresponds to the usual interpretation of interference effects as being due to the autoionization of a (quasi-) discrete parabolic channel coupled to one (or more) continuum channels of lower n_1 which provide the background. Note, however, that the continua intensity enter into Eqs. (77) as *constant* terms, whereas all odd or even variations in amplitude near a resonance are contained here in the parameters R^{-2} and $R^{-2}\cot\gamma$ of the resonant channel itself. This differs from Fano's treatment[24] of configuration interactions, inasmuch as wave functions of *different* channels are coupled through an interaction Hamiltonian V_ε. Here the parabolic continua play two separate roles: (1) the wave function of a quasidiscrete state of the inner potential well at $\eta \ll F^{-1/2}$ [see Fig. 6(c)] is "coupled" *through the potential barrier* to the continuum region $\eta \gg F^{-1/2}$ of the *same wave function at the same energy,* producing variations in the amplitude $R_{\bar{\beta}}^F$ and the phase shift $\gamma_{\bar{\beta}}^F$; (2) the greatest intensities come in Eq. (61) from those channels $\beta \neq \bar{\beta}$ ($n_1 < \bar{n}_1$) whose wave functions are above the top of their respective potential barriers ($R_{\bar{\beta}}^F \sim 1$), as in Fig. 6(a), and which we may characterize as "continua" in the region $\eta \ll F^{-1/2}$. Both kinds of parabolic continua are coupled to the quasidiscrete state by the spherical but nonhydrogenic core, represented by δ_l in Eq. (58).

2. Limit $F \to 0$

Finally, we verify that the cross section $\sigma_{l'l}^F$ actually reduces to its zero-field alkali-metal spectrum

as $F \to 0$. Above threshold, we know that $\tilde{U} \to U^{-1}$ and $H^F \to 1$ [Eq. (18)] and that $h^F \to 0$ [all $\gamma_\beta^0 \to \frac{1}{2}\pi$], so Eq. (58) for D^F trivially reduces to the identity matrix. Below threshold, we consider that all parabolic channels have degenerate energy eigenvalues when $F \to 0$; then Eq. (60) becomes

$$H_{l'l}^F = \sum_\beta (\tilde{U}_{l'\beta}^0 U_{\beta l}^0) \left| \left\{ \frac{(\frac{1}{2}\Gamma_\beta/\pi)}{(\varepsilon - \varepsilon_0)^2 + (\frac{1}{2}\Gamma_\beta)^2} \frac{d\varepsilon}{dv} \right\}_{v_0} \right| , \tag{90}$$

where $\varepsilon_0 = -\frac{1}{2}v_0^{-2}$, $v_0 = n_1 + n_2 + m + 1$, $n_1 = 0, 1, 2, \ldots,$ and

$$d\varepsilon/d(\Delta/\pi) = d\varepsilon/dn_2 = d\varepsilon/dv$$

is the same for all channels. Moreover, every value of Γ_β (or $1/\Gamma_\beta$) is exponentially small (or large) so with negligible error at either $\varepsilon = \varepsilon_0$ or $\varepsilon \neq \varepsilon_0$ we may factor out a common Lorentzian from Eq. (90) with $\Gamma_\beta = \Gamma$. The bracketed factor in Eq. (90), R^{-2}, then approaches the δ function $\delta(v - v_0)$ as $\Gamma \to 0$ [cf. Eq. (63)], while by Eq. (18) the transformation $U_{\beta l}^0$ becomes orthogonal. Similarly, $h_{l'l}^F$ approaches the form (90) with $(\frac{1}{2}\Gamma/\pi)$ replaced by $(\varepsilon_0 - \varepsilon)/\pi$ and we are left with unit matrices multiplied by

$$H^F \underset{F \to 0}{\to} R^{-2}, \quad h^F \underset{F \to 0}{\to} R^{-2}\cot\gamma \ . \tag{91}$$

When these are inserted into Eq. (58), $D_{l'l}^F$ reduces to a diagonal matrix whose elements resemble Eq. (78) with $\delta_l' = \delta_l$ and $\Delta = \pi(n_2 + \frac{1}{2})$:

$$D_{II}^F = R'^{-2} = [\ T^2\sin^2\pi(n_2 + \mu_l)$$
$$+ T^{-2}\cos^2\pi(n_2 + \mu_l)]^{-1} \ . \tag{92}$$

This result is identical to Eq. (89) with $B = b = 0$, $c = 1$, and $\delta_l' = \delta_l$ from Eqs. (77) and (91). In the limit $T^{-2} \to 0$, Eq. (92) becomes $D_{II}^F = \delta(v_0 + \mu_l - n)$ for integral n. Thus at $F \to 0$ the modulating factor singles out the proper discrete levels $\varepsilon = -\frac{1}{2}(n - \mu_l)^{-2}$, in analogy to Eq. (18) for H,

and the cross section reduces to its proper form (24) with n replaced by $n^* = n - \mu_l$.

IV. COMPARISON WITH EXPERIMENTS NEAR THRESHOLD

Experiments have been reported on Rb and Na in electric fields near the zero-field ionization limit. We consider here only the sodium experiments, all of which involve two-photon excitation. The available experimental data on photoabsorption by Na in a Stark field consists of the work of three groups: (1) Luk, DiMauro, Bergeman, and Metcalf,[3] (2) Feneuille et al.,[4] and (3) Sandner, Safinya, and Gallagher.[5] For purposes of comparing theoretical cross sections with experiments we consider their results in turn.

(1) In Ref. 3, Na atoms in the ground state were ionized by two photons, polarized $\pi\pi$, through the 3^2P_j intermediate state. The first laser was tuned to either the $j = \frac{3}{2}$ or $\frac{1}{2}$ state of the Na D line, whose

splitting (17 cm^{-1}) far exceeds the laser resolution (0.3 cm^{-1}). Since the second ionizing laser was pulsed simultaneously with the first and since the laser pulses occur on a shorter time scale (10 nsec) than hyperfine transitions, we will ignore here hyperfine effects on the fine structure 3^2P_j state. In order to apply the procedures of Sec. III, we need to expand the ls-coupled intermediate state $|j, m_j\rangle$ in an $|l, m_l\rangle |s, m_s\rangle$ basis for $j = \frac{3}{2}$ or $\frac{1}{2}$, $m_j = \pm \frac{1}{2}$, $s = \frac{1}{2}$, $m_s = \pm \frac{1}{2}$, and $l = 1$:

$$|\tfrac{3}{2}, \pm\tfrac{1}{2}\rangle = (\tfrac{2}{3})^{1/2} |1,0\rangle |\tfrac{1}{2}, \pm\tfrac{1}{2}\rangle$$
$$+ (\tfrac{1}{3})^{1/2} |1, \pm 1\rangle |\tfrac{1}{2}, \mp\tfrac{1}{2}\rangle , \quad (93a)$$

$$|\tfrac{1}{2}, \pm\tfrac{1}{2}\rangle = (\tfrac{1}{3})^{1/2} |1,0\rangle |\tfrac{1}{2}, \pm\tfrac{1}{2}\rangle$$
$$- (\tfrac{2}{3})^{1/2} |1, \pm 1\rangle |\tfrac{1}{2}, \mp\tfrac{1}{2}\rangle . \quad (93b)$$

Entering these initial states for Ψ_i in Eqs. (56) and (57) (with $l=2$, $l'=0$) we obtain the $\pi\pi$ cross sections

$$\sigma_{3/2}^F(\epsilon) = \tfrac{2}{3}\{\sigma^F(\epsilon), m = 0 \to 0\} + \tfrac{1}{3}\{\sigma^F(\epsilon), m = 1 \to 1\} , \tag{94a}$$

$$\sigma_{1/2}^F(\epsilon) = \tfrac{1}{3}\{\sigma^F(\epsilon), m = 0 \to 0\} + \tfrac{2}{3}\{\sigma^F(\epsilon), m = 1 \to 1\} , \tag{94b}$$

where we have indicated the second π transition by $m_i \to m_f = m_i$. Thus, ls coupling simply superposes the cross sections with $m_f = 0$ and $m_f = 1$, thereby mixing two sets of resonances. According to Fig. 5 for H—as an approximation to Na—Eqs. (94) should also have the effect of superposing relatively large $m = 0 \to m = 0$ threshold modulations with the relatively flat $m = 1 \to m = 1$ spectrum.

Figure 8(a) shows an experimental photoionization spectrum[25] of Na $3^2P_{3/2}$ from Ref. 3, with $F = 3.59$ kV/cm $= 6.98 \times 10^{-7}$ a.u. Figure 8(b) shows the results of a calculation using the present theory. In our calculation of $\sigma_{3/2}^F$, Eq. (94a), we used the first and third expressions of of Table II; $H_{l'l}^F$ was replaced by $D_{l'l}^F$, Eq. (58), using hydrogenic parameters $N_{\epsilon n_1 m}^F$ and $\beta_{\epsilon n_1 m}^F$ calculated[10] for $n_1 = 0 - 30$ and the values of the quantum defects cited in Eq. (59). The zero-field radial dipole matrix elements for Na used in Eq. (57), $R_{31}^{\epsilon d}$ and $R_{31}^{\epsilon s}$, were extrapolated through threshold from a theoretical calculation for high Rydberg states,[26] which appears more reliable than existing experimental data[14] for the Na $3p \to ns$ transitions.

The theoretical spectrum of Fig. 8(b) reproduces both the positions and shapes of the resonances observed below threshold. We can account for the res-

onance profiles on the basis of the discussion of Figs. 3 and 4 in Sec. III C. The sharp resonances contributed by $\{\sigma^F(\epsilon), m = 1 \to m = 1\}$—marked by $m_l = 1$ in Fig. 8(a)—are little changed by the Na core from their hydrogenic Stark spectrum: as in Fig. 4(a) for $m = 1$, the small value of $\mu_2 = 0.014$ does not broaden the peaks in the modulating factor D_{22}^F significantly from H_{22}^F. The sharper peaks are broadened, however, by experimental limitations.

The pronounced asymmetry of the $m_l = 0$ resonances follows from the properties of the DOS matrix elements D_{00}^F, D_{20}^F, and D_{22}^F for Na, shown for a larger field in Figs. 3(a)–3(c). For example, the sharp $(11,10,0,0)$ peak is broadened and has the same asymmetry sign in each spectrum, the asymmetry being determined by Eq. (72) with the quantum defects (59). The modulating factors are admixed in the cross section (56) in the ratio $D_{00}^F : D_{20}^F : D_{22}^F \approx 1.0 : 3.1 : 2.4$, according to Table II(a) for $\pi\pi$ polarization (note that D_{20}^F enters with a $+$ sign). Thus, both D_{00}^F and the interference term D_{20}^F are responsible for the asymmetric line shapes in Fig. 8. For $m = 0$ resonances obtained via $\sigma^+\sigma^-$ polarization, D_{20}^F would enter σ^F with the opposite sign and we would expect the asymmetry to be reversed. This effect has indeed been observed[4] in
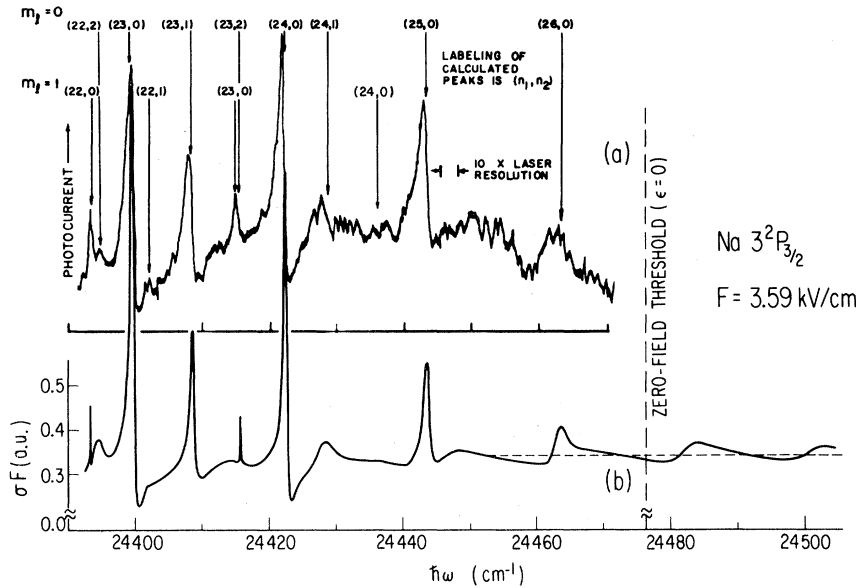
FIG. 8. (a) Experimental $\pi\pi$ photoionization spectrum of Na $3^2P_{3/2}$ in a field $F=3.59$ kV/cm, vs photon energy $\hbar\omega$, within 0.01 eV of threshold (Ref. 2). Note labeling of Stark resonances (n_1,n_2) for $m_l=0$ and 1. (b) Theoretical cross section, Eqs. (56)—(58); ---- $\sigma^{F=0}$. Asymmetric peaks labeled as for (a) and discussed in the text. Stark-induced oscillations for $m_l=0$ extend past $\epsilon=0$ with same spacing as in H (19.6 cm^{-1}) and 11% depth of modulation.

another spectrum and is discussed below. The Fano parameters for the $m_l=0$ peak at $\hbar\omega=24\,422$ cm^{-1} in Fig. 8(a), labeled (24,0), have been measured[3] as $q=-1.7(0.3)$ and $\Gamma=0.7(0.15)$ cm^{-1}. The values of these parameters taken from the theoretical spectrum in Fig. 8(b) are $q=-3.3$ and $\Gamma=0.39$ cm^{-1}, corresponding to a sharper peak unbroadened by experimental resolution. However, we obtain the values $q=-2.6$ and $\Gamma=0.82$ cm^{-1} when the lattice spectrum is folded into a Gaussian distribution corresponding to a resolution of $\Gamma_{exp}=0.6$ cm^{-1}. The calculated depth of the modulations at $\epsilon\gtrsim0$ is 11%, which exceeds the experimental value $[(6\pm2)\%]$.

(2) In Ref. 4, Na atoms were first optically pumped from the ground state to the $3^2P_{3/2}$, $F=M_F=3$ hyperfine level by a circularly (σ^+) polarized cw laser. This pure $m_l=1$ state was then ionized in a Stark field $F=9950$ V/cm by a σ^--, π-, or σ^+-polarized dye laser, yielding final states with $m_l=0,1$, or 2. The calculated spectra for these polarizations, shown in Figs. 9(a)—9(c) versus wavelength, are to be compared with the experimental data in Figs. 2(a'), (b'), and (c') of Ref. 4. Again, the theory reproduces both the shapes and positions of the resonances below threshold, labeled by (n,n_1) in Fig. 9.

(a) The $m_l=0$ $(\sigma^+\sigma^-)$ spectrum [Fig. 9(a)] displays broad, highly asymmetric peaks like those in Fig. 8 for $\pi\pi$ polarization. The resonances in

Fig. 9(a), however, are asymmetric in the opposite sense and not as sharp. As anticipated above, this is because the DOS cross term D_{20}^F enters into Eq. (56) with a negative coefficient (cf. the second expression of Table II).

(b) The $m_l=1$ $(\sigma^+\pi)$ resonances [Fig. 9(b)] are only slightly asymmetric with $q<0$, owing to the small value of μ_2 in Eq. (86'). The single matrix element D_{22}^F also depends on μ_1, whose effect is only to broaden the peaks slightly [cf. Fig. 7(d)].

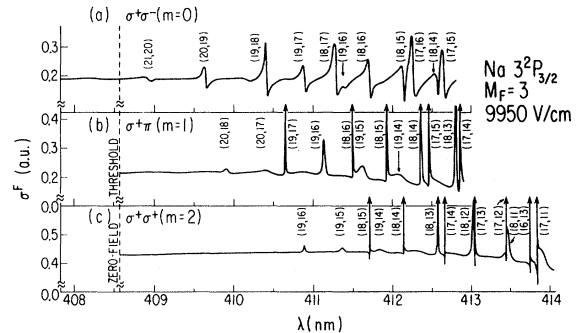(c) The $m_l=2$ $(\sigma^+\sigma^+)$ spectrum [Fig. 9(c)] is

FIG. 9. Theoretical cross sections for photoionization of Na $3^2P_{3/2}$, $F=M_F=3$, $m_l=1$, in a field 9950 V/cm, vs wavelength λ. Polarizations (a) σ^- $(m=0)$, (b) π $(m=1)$, (c) σ^+ $(m=2)$. Stark resonances labeled by (n,n_1); different peak asymmetries for (a)—(c) discussed in the text. Experimental spectra appear in Fig. 4.

given exactly by Eq. (73) for D_{22}^F. The peaks are very sharp and essentially hydrogenic, i.e., $q \ll -1$. The interference dips are apparent—even though $|q| \approx 25$—only because the peaks are so narrow, but all the sharp features in Fig. 9(c) are anyhow broadened in the experimental spectrum.

(3) The Na experiments of Ref. 5 are similar to those of Ref. 3, except that spectra were observed for intermediate 3^2P_j states with both $j = \frac{3}{2}$ and $\frac{1}{2}$ in a field $F = 8.91$ kV/cm. Our theory reproduces these results as well, but we do not display the calculated spectra. The predicted depth of modulations above thresholds, 18% for $j = \frac{3}{2}$ and 11% for $j = \frac{1}{2}$, agree with the observed values.

As far as computation is concerned, to a 0.1% level of accuracy,[10] the use of semianalytical WKB parameters for the hydrogen-Stark wave functions is very efficient. Each of the spectra shown in Figs. 8 and 9(a)—9(c) were calculated on an IBM 370 computer in 20—30 sec of CPU (central-processing unit) time.

V. CONCLUDING REMARKS

Our treatment of photoionization in this paper should in fact be applicable to phenomena other than the Stark effect. We have considered separately (a) the localized photoabsorption process for zero field and (b) the effects of long-range fields on the photoelectron's density of states. The DOS matrix $D^F = \langle \Psi' | \Psi \rangle^{-1}$ contains the parameters H^F and h^F, but these parameters do not depend explicitly on details of the asymptotic channels, such as the continuous or discrete nature of their spectra or the coordinate system used. Accordingly, our formulation should be essentially applicable to the quadratic Zeeman effect, whenever it would be possible to construct the analogs of H^F and h^F. Our analysis is also applicable, e.g., to molecular photoabsorption by simply allowing for the greater variety of channels corresponding to ionization, rovibrational excitation, and photodissociation.

ACKNOWLEDGMENTS

APPENDIX A: HYDROGENIC WKB PARAMETERS

We collect here the WKB expressions for the hydrogenic parameters used in our calculations, most of which are given in detail in Ref. 10.

For fixed F, m, and ϵ the eigenvalues $\beta_{\epsilon n_1 m}^F$ are determined by the quantization condition (5) in ξ, with $n_1 = 0, 1, 2, \ldots$. If the eigenfunctions $\Xi_\beta^F(\xi)$ of Eq. (3a) are normalized at $\xi \sim 0$ (1 a.u.) as Coulomb functions, they must be further normalized for $F \neq 0$ by the factor

$$N_\xi = \left[\frac{1}{\pi} \int_a^b \frac{d\xi'}{k(\xi')\xi'} \right]^{-1/2} , \qquad (A1)$$

where the WKB wave number $k(\xi)$ appears in Eq. (5) and a and b are its two non-negative roots. We have assumed in Eq. (A1) that $\Xi_\beta^F(\xi \gg 1)$ has the WKB form (33a) and that $\sin^2(\cdots) \approx \frac{1}{2}$ on the average. Note that N_ξ may be interpreted as a renormalization amplitude from a smooth to a discrete spectrum in the eigenvalue β at fixed ϵ, i.e.,

$$N_\xi^2 = \frac{d\beta_{\epsilon m}^F}{dn_1} \bigg|_{\beta = \beta(\epsilon, F; n_1, m)} . \qquad (A2)$$

In this sense N_ξ^2 measures the spacing in the smoothly varying parameter $\beta_{\epsilon m}^F$ between discrete states with n_1 and $n_1 \pm 1$ nodes, just as $d\epsilon/dn = n^{-3}$ in Eq. (8) represents the spacing between hydrogenic levels at fixed Z or β. If the levels are closely spaced then $\sum_{n_1=0}^N$ may be replaced by $\int d\beta$, with an error $\sim O(1/N)$.

In the unbound coordinate, the wave functions $\Upsilon_\beta^F(\eta)$ and $\overline{\Upsilon}_\beta^F(\eta)$ normalized at $\eta \ll F^{-1/2}$ as in Eqs. (33a) and (33b) acquire barrier-penetration amplitudes R_β^F and S_β^F at $\eta \to \infty$ (we assume here $\beta_2 = 1 - \beta > 0$). In a generalized WKB method[27] which allows for two propinquous turning points we define (1) the WKB phase accumulated in the potential well of Fig. 6,

$$\Delta = \text{Re} \int_c^b k(\eta')d\eta' , \qquad (A3)$$

$$k(\eta) = \left[-\frac{m^2}{4\eta^2} + \frac{1-\beta}{\eta} + \frac{1}{2}\epsilon + \frac{1}{4}F\eta \right]^{1/2} , \qquad (A4)$$

and (2) the tunneling integral

$$\tau = \mathrm{Im} \int_b^a k(\eta')d\eta' , \qquad \text{(A5)}$$

where the turning points $c < b \leq a$ are real if $\epsilon \leq \epsilon_c$ and b and $a = b^*$ are complex $(c < \mathrm{Re}b)$ if $\epsilon > \epsilon_c$. Thus defined, Δ and τ are real quantities which vary smoothly through the barrier top and which account for reflection from the barrier; note, moreover, that $\tau \gtrless 0$ for $\epsilon \lessgtr \epsilon_c$. The amplitude R_β^F is

$$R_\beta^F = (T^2\cos^2\Delta + T^{-2}\sin^2\Delta)^{1/2} , \qquad \text{(A6)}$$

where

$$T = (1 + e^{2\tau})^{1/2} + e^\tau ; \qquad \text{(A7)}$$

S_β^F is obtained from R_β^F by substituting $\Delta \rightarrow \Delta - \frac{1}{2}\pi$:

$$S_\beta^F = (T^2\sin^2\Delta + T^{-2}\cos^2\Delta)^{1/2} . \qquad \text{(A8)}$$

At (a) $\epsilon \ll \epsilon_c$ $(\tau \gg 0)$ and (b) $\epsilon \gg \epsilon_c$ $(\tau \ll 0)$, T approaches the familiar limiting WKB cases of (a) two well-separated turning points, $T \rightarrow 2e^\tau$, and (b) a single classical region without reflection above the barrier top, $T \rightarrow 1$. In the latter case, both R_β^F and $S_\beta^F \rightarrow 1$ independently of Δ. Below the barrier (with $T \gg 1$), $(R_\beta^F)^{-2}$ is a normalized Lorentzian in the variable $(\Delta/\pi) - \frac{1}{2}$, centered at $\Delta \mod(\pi) \approx \frac{1}{2}\pi$ $(\epsilon = \epsilon_0)$, and with full width at half maximum $\Gamma = 2T^{-2}/\pi \ll 1$; in the energy variable ϵ, $(\Delta/\pi) - \frac{1}{2}$ is replaced by $(\epsilon - \epsilon_0)d(\Delta/\pi)/d\epsilon$, as in Eq. (63). In the limit $T^{-2} \rightarrow 0$, $(R_\beta^F)^{-2} \rightarrow \delta(\Delta/\pi - n)$, with an n half-integral.

The asymptotic relative phase shift γ_β^F between $\Upsilon_\beta^F(\eta \rightarrow \infty)$ and $\widetilde{\Upsilon}^F(\eta \rightarrow \infty)$ follows from the Wronskian (47) and Eqs. (A6) and (A8):

$$\cot\gamma_\beta^F = [(R_\beta^F S_\beta^F)^2 - 1]^{1/2}$$
$$= (T^2 - T^{-2})\sin\Delta \cos\Delta, \quad 0 < \gamma_\beta^F < \pi .$$
$$\text{(A9)}$$

For $\epsilon < \epsilon_c$, γ_β^F is confined to $\gtrsim 0$ or $\lesssim \pi$, except when $2\Delta \approx 0 \pmod{\pi}$. For $\epsilon > \epsilon_c$,

$$\gamma_\beta^F \rightarrow \frac{1}{2}\pi - e^{-|\tau|}\sin2\Delta \underset{\tau \rightarrow -\infty}{\longrightarrow} \frac{1}{2}\pi .$$

APPENDIX B: MATRIX ALGEBRA FOR D^F.

The DOS matrix D^F is an inverted overlap matrix, given in its most general form in Eq. (58). In the hydrogenic limit with $\delta_l = 0$ the overlap (25) is simply $(H^F)^{-1}$, which upon inversion gives $D_{l'l}^F = H_{l'l}^F$. However, the factors in Eq. (58) con-

taining $\sin\delta \neq 0$ (and $\cos\delta \neq 1$) complicate this picture and $D_{l'l}^F$ apparently involves the entire matrices H^F and $(H^F)^{-1}$ rather than a single matrix element. Nevertheless, the actual effect of having only a few nonvanishing elements of the diagonal matrix $\sin\delta$ is to supplement $H_{l'l}^F$ only by the few matrix elements $H_{l'l}^F$ and $h_{l'l}^F$ with $\delta_{l'}$ or $\delta_l \neq 0$. We show this by reducing the inversions in D^F to a finite eigenvalue problem, as follows.

We first proceed without specifying whether δ_l vanishes and define the matrix

$$Q = 1 - h^F\tan\delta , \qquad \text{(B1)}$$

where 1 is the identity matrix and $\tan\delta$, $\sec\delta$, etc., are diagonal. Then with $H^F = \widetilde{U}U$ the symmetric expression (58) becomes

$$D^F = \sec\delta \, Q^{-1}$$
$$\times \widetilde{U}[1 + (U\widetilde{Q}^{-1}\tan\delta \, \widetilde{U})(U\tan\delta \, Q^{-1}\widetilde{U})]^{-1}$$
$$\times U\widetilde{Q}^{-1}\sec\delta . \qquad \text{(B2)}$$

The symmetric matrix in parentheses in Eq. (B2) is diagonalized by an orthogonal matrix $B = \widetilde{B}^{-1}$ with eigenvalues Λ_λ,

$$U\widetilde{Q}^{-1}\tan\delta \, \widetilde{U} = B\Lambda B^{-1} . \qquad \text{(B3)}$$

Inserting this expression into Eq. (B2), we obtain

$$D^F = \sec\delta \, W(1 + \Lambda^2)^{-1}\widetilde{W}\sec\delta , \qquad \text{(B4)}$$

where we have defined the unsymmetric matrix

$$W = Q^{-1}\widetilde{U}B . \qquad \text{(B5)}$$

(The elements of both B and W are labeled by indices $l, \lambda = 0, 1, \ldots$.) Now we see from Eqs. (B3) and (B5) (and the transposition relation $\widetilde{Q}^{-1}\tan\delta = \tan\delta \, Q^{-1}$) that W diagonalizes the matrix $Q^{-1}\widetilde{U}U\tan\delta$ with the same eigenvalues Λ_λ, i.e.,

$$(1 - h^F\tan\delta)^{-1}H^F\tan\delta = W\Lambda W^{-1} . \qquad \text{(B6)}$$

Since the left-hand side (lhs) of Eq. (B6) is not symmetric, W is nonorthogonal; the eigenvectors W_λ forming its columns are instead normalized by first rewriting Eq. (B5) as

$$W\widetilde{W} = (1 - h^F\tan\delta)^{-1}H^F(1 - \tan\delta \, h^F)^{-1} \qquad \text{(B7)}$$

and then using Eq. (B3) to obtain

$$(\widetilde{W}\tan\delta \, H^F\tan\delta \, W)_{\lambda'\lambda} = \Lambda_\lambda^2 \delta_{\lambda'\lambda} . \qquad \text{(B8)}$$

Recalling that $H^F \rightarrow 1$ and $h^F \rightarrow 0$ for $F \rightarrow 0$, these equations show that $W \rightarrow 1$ and $\Lambda \rightarrow \tan\delta$ in that limit; accordingly we regard Λ as the generalization

of the reaction matrix of the core, $-\pi K = \tan\delta$, for $F\neq 0$.

The DOS matrix D^F is thus expressed in Eq. (B4) through the eigenvalue problem (B6) with the normalization conditon (B8). Equation (B4) simplifies under the realistic requirement that

$$\delta_l\neq 0, \quad l=0,1,\ldots,N-1\lesssim 3 \tag{B9a}$$

$$\delta_l=0, \quad l\geq N . \tag{B9b}$$

The factor $\tan\delta$ sets to zero all but the first N columns of both $h^F\tan\delta$ and $H^F\tan\delta$ in Eq. (B6), thus permitting a straightforward inversion of $1-h^F\tan\delta$. The diagonalization of the lhs of (B6) will then determine at most N nonvanishing eigen-

values Λ_λ, $\lambda=0,1,\ldots,N-1$, so our eigenvalue problem is in fact confined to the $N\times N$ subspace where $\delta_l\neq 0$. The portion of Λ outside this subspace vanishes and $W_{l\lambda}$ and Λ_λ for $l,\lambda<N$ depend *only* on those matrix elements $H^F_{l'l}$ and $h^F_{l'l}$ with $l',l<N$.

Our final expression for $D^F_{l'l}$ will depend on whether the specific indices l' and l fall within the range (B9a) or (B9b). If both $l'<N$ and $l<N$, $D^F_{l'l}$ is given just by Eq. (B4) with $\lambda<N$. If either $l'\geq N$ or $l\geq N$, we use Eq. (B6) to find the components $W_{l\lambda}$ $(l\geq N)$ of the eigenvectors W_λ $(\lambda\leq N)$. We then write Eq. (B4) explicitly as a sum over $\Lambda_\lambda\neq 0$, using $(1+\Lambda^2)^{-1}=1-\Lambda^2/(1+\Lambda^2)$:

$$\begin{aligned}
D^F_{l'l}= {}& [(\cos\delta-h^F\sin\delta)^{-1}H^F(\cos\delta-\sin\delta\, h^F)^{-1}]_{l'l}\\
& -\sec\delta_{l'}\left[\sum_{\lambda=0}^{N-1} W_{l'\lambda}\frac{\Lambda_\lambda^4(1+\Lambda_\lambda^2)^{-1}}{[\widetilde{W}\tan\delta\, H^F\tan\delta\, W]_\lambda}\widetilde{W}_{\lambda l}\right]\sec\delta_l ,
\end{aligned} \tag{B10}$$

where we have used Eq. (B7) for $W\widetilde{W}$ and Eq. (B8) for initially unnormalized W_λ. The first term in Eq. (B10) corresponds to the expression (58) without the term $\sin\delta\, H^F\sin\delta$ and thus represents a generalization of the hydrogenic form (27), $D^F_{l'l}=H^F_{l'l}$. The sum over eigenvalues in Eq. (B10) stems instead from the second term in (58) itself—through the squared matrix (B3) appearing in Eq. (B2) and

hence through Λ^2—and represents, loosely speaking, the admixture of irregular functions $\chi^F_\beta(\vec{r})$ into $\Psi_l(\vec{r})$ in Eqs. (53) and (54). Therefore, we see that the presence of nonzero values of $\tan\delta_l$ in the wave functions (35) and in the DOS matrix (58) brings into the expressions (B4) and (B10) for D^F only the nonzero matrix elements of $h^F\tan\delta$ and $H^F\tan\delta$ from Eq. (B6).

*Present address: National Bureau of Standards, Phys. A-153, Gaithersburg, Maryland 20760.

[1](a) R. R. Freeman, N. P. Economou, G. C. Bjorklund, and K. T. Lu, Phys. Rev. Lett. **41**, 1463 (1978); (b) R. R. Freeman and N. P. Economou, Phys. Rev. A **20**, 2356 (1979).

[2]S. Feneuille, S. Liberman, J. Pinard, and A. Taleb, Phys. Rev. Lett. **42**, 1404 (1979).

[3]T. S. Luk, L. DiMauro, T. Bergeman, and H. Metcalf, Phys. Rev. Lett. **47**, 83 (1981).

[4]S. Feneuille, S. Liberman, E. Luc-Koenig, J. Pinard, and A. Taleb, Phys. Rev. A **25**, 2853 (1982); S. Liberman (private communication).

[5]W. Sandner, K. A. Safinya, and T. F. Gallagher, Phys. Rev. A **23**, 2448 (1981).

[6]M. Nayfeh (unpublished).

[7](a) B. E. Cole, J. W. Cooper, and E. B. Saloman, Phys. Rev. Lett. **45**, 887 (1980); (b) J. W. Cooper and E. B. Saloman, Phys. Rev. A **26**, 1452 (1982).

[8]A. R. P. Rau, J. Phys. B **12**, L193 (1979).

[9](a) E. Luc-Koenig and A. Bachelier, J. Phys. B **13**, 743 (1980); (b) *ibid.* **13**, 1769 (1980); (c) Phys. Rev. Lett. **43**, 921 (1979).

[10]D. A. Harmin, Phys. Rev. A **24**, 2491 (1981), referred to as I.

[11]V. D. Kondratovich and V. N. Ostrovskii, Zh. Eksp. Teor. Fiz. **79**, 395 (1980) [Sov. Phys.—JETP **52**, 198 (1981)].

[12]D. A. Harmin, Phys. Rev. Lett. **49**, 128 (1982).

[13]U. Fano, Phys. Rev. A **24**, 619 (1981). The extension of angular momentum recoupling to include complex eigenvalues, emphasized in this paper, follows from W. J. Holman III and L. C. Biedenharn, Jr., Ann. Phys. (N.Y.) **39**, 1 (1966).

[14]W. L. Wiese, M. W. Smith, and B. M. Miles, *Atomic Transition Probabilities II*, Natl. Stand. Ref. Data Service, Natl. Bur. Stand. (U.S), 22 (U.S. GPO, Washington, D.C., 1969).

[15]H. A. Bethe and E. E. Salpeter, *Quantum Mechanics of One- and Two-Electron Atoms* (Springer, Berlin, 1957), Secs. 1—4 and 6.

[16]L. D. Landau and E. M. Lifshitz, *Quantum Mechanics (Non-Relativistic Theory)* (Pergamon, Oxford, 1976), 3rd ed., Secs. 36 and 37.

[17]See Sec. VIII of M. L. Zimmerman, M. G. Littman, M. M. Kash, and D. Kleppner, Phys. Rev. A **20**, 2251

(1979), where the high-lying Stark-Rydberg states of alkalis are calculated in a spherical basis adapted to the core. See also Ref. 7(b).

[18]C. H. Greene, U. Fano, and G. Strinati, Phys. Rev. A 19, 1485 (1979); C. H. Greene, A. R. P. Rau, and U. Fano, Phys. Rev. A (in press).

[19]See Ref. 15, Secs. 51—54 and Ref. 16, Sec. 77.

[20]See especially Eqs. (22), (38), (54), and (64) of Ref. 10.

[21]See, e.g., D. R. Herrick, Phys. Rev. A 12, 1949 (1975) and references therein.

[22]See, e.g., p. 262 of Ref. 15. Note that their general expression for $R_{nl}^{n'l-1}$, Eq. (63.2), must be multiplied by $(dv/d\epsilon)^{1/2} = v^{3/2}$, in accordance with our normalization Eq. (8).

[23]C. E. Moore, *Atomic Energy Levels I—III*, Natl. Bur. Stand. (U.S.) Circ. No. 467 (U.S. GPO, Washington, D.C., 1971).

[24]U. Fano, Phys. Rev. 124, 1866 (1961).

[25]Note that Fig. 2 of Ref. 3 incorrectly marks the zero-field ionization threshold, 24476 cm^{-1}, at ≈ 24471 cm^{-1} (dashed line).

[26]K.-T. Cheng (private communication). The dipole matrix elements for $3p \to ns$ and nd transitions in Na ($n = 9-14$) have the approximate linear dependence on ϵ (in a.u.):

$$R_{31}^{n0} = 3.32 - 53.9\epsilon \ ,$$

$$R_{31}^{n2} = 5.79 - 152.2\epsilon \ .$$

[27]S. C. Miller and R. H. Good, Jr., Phys. Rev. 91, 174 (1953); Ref. 10, Appendix A.